The impact of circulating tumor DNA in biliary tract cancer under chemotherapy

WOOBIN YUN

Department of Medical Science

The Graduate School, Yonsei University

The impact of circulating tumor DNA in biliary tract cancer under chemotherapy

Directed by Professor JONG RAK CHOI

The Doctoral Dissertation
submitted to the Department of Medicine,
the Graduate School of Yonsei University
in partial fulfillment of the requirements for the degree of
Doctor of Philosophy in Medical Science

WOOBIN YUN

December 2022

This certifies that the Doctoral Dissertation of WOOBIN YUN is approved.

Thesis Supervisor: JONG RAK CHOI

Thesis Committee Member#1: SEUNG-TAE LEE

Thesis Committee Member#2: HYO SUP SHIM

Thesis Committee Member#3: CHOONG-KUN LEE

Thesis Committee Member#4: JIEUN KIM

The Graduate School
Yonsei University

December 2022

ACKNOWLEDGEMENTS

I would like to express my gratitude to all those who gave me the possibility to complete this thesis. First, I appreciate my supervisor, **Prof. Jong Rak Choi** who supported me to finish all work. I sincerely appreciate **Prof. Seung-Tae Lee**, **Prof. Choong-Kun Lee**, **Prof. Hyo Sup Shim**, and **Prof. Jieun Kim** who give me a lot of good advice for my research. Also, thanks to **Prof. Sae Am Shin** and **Ph.D. Jieun Seo** who offered guidance and support. I am grateful to my colleagues, **Hyeon Ah Lee**, **Miri Park**, **Yeeun Shim**, and **Taek Gyu Lee**, who encouraged me to go the distance.

I am indebted to so many, but I especially wish to acknowledge the efforts and encouragement of my family. I thank my parents and sister for their continued love and support.

I would not have been able to achieve my Ph.D. degree without their support.

Woobin Yun
Yonsei University College of Medicine
December 2022

<TABLE OF CONTENTS>

LIST OF FIGURES

LIST OF TABLES

ABSTRACT

The impact of circulating tumor DNA in biliary tract cancer under chemotherapy

WOOBIN YUN

Department of Medical Science
The Graduate School, Yonsei University

(Directed by Professor JONG RAK CHOI)

Biliary tract cancer (BTC) is a highly aggressive cancer with a very poor prognosis. In general, the incidence of BTC is higher in Eastern countries than in Western countries. BTC was once considered a geographically region-specific disease. However, according to recent reports, the incidence of BTC has increased globally. Most patients with BTC were first diagnosed at the advanced stage because the disease is usually asymptomatic during the early stage. Tissue biopsy is the current gold standard for cancer diagnosis, but this invasive technique has challenges. Despite the increased incidence rate and poor prognosis of BTC, understanding this disease is still not satisfactory. To discover actionable target genes and monitor the drug response of patients, we enrolled unresectable BTC patients (n = 41), and circulating-tumor DNA (ctDNA) from plasma samples was collected at multiple timepoints while patients received chemotherapy (pre-1st chemotherapy, pre-2nd chemotherapy, pre-4th chemotherapy, and progression disease). All samples were deep sequenced with a large panel containing 531 pan-cancer genes. We identified highly observed variants, such as *TP53*, *ARID2*, *KRAS*, *ARID1A*, *PDE4DIP*, *ARID1B*, *CHD4*, *FAT1*, *PIK3CA*, *SPEN*, *APC*, *ATM*, *ATR*, *ERBB4*, *FGFR2*, and *IDH1*. In addition, copy number alterations (CNAs) of *MYC*, *ERBB2*, *CDKN2A*, *GATA4*, *ARID2*, *MDM2*, *PIK3R3*, *CDK12*, and *EGFR* were observed. Key pathways and genes were curated from the literature and detected single nucleotide variants (SNVs) were categorized by them. Epigenetic regulation, TP53 signaling, the PI3K/AKT/mTOR and RAS/RAF/ERK

pathways, DNA damage, angiogenesis, and DNA repair were highly ranked. *TP53*, *ARID2*, and *PTPRT* frequently occurred under chemotherapy. In particular, the *PTPRT* mutation remarkably increased in a cohort with progression disease as compared with that of cohorts at other timepoints. The survival rate of BTC patients with a low tumor mutation burden (TMB) was higher than that of the high TMB patient group. Also, a new threshold by delta blood TMB (dTMB) showed potential as a marker for diagnosis. In the present study, we suggested the advantages of cell-free DNA (cfDNA)-targeted sequencing and discussed candidates of precision therapy and understanding molecular profiling of BTC patients under chemotherapy.

Key words : biliary tract cancer, cholangiocarcinoma, chemotherapy, cell-free DNA, circulating-tumor DNA, next-generation sequencing, liquid biopsy

The impact of circulating tumor DNA in biliary tract cancer under chemotherapy

WOOBIN YUN

Department of Medical Science
The Graduate School, Yonsei University

(Directed by Professor JONG RAK CHOI)

I. INTRODUCTION

Biliary tract cancer (BTC) is a malignant cancer in epithelial cells of the bile duct. It is composed of three main types based on anatomical location: gallbladder carcinoma (GBC), intrahepatic cholangiocarcinoma (IHCCA), and extrahepatic cholangiocarcinoma (EHCCA)[1]. Although GBC is generally considered rare, it is the most common BTC malignancy type and shows a high incidence rate (80-95 %) in BTC[2]. BTC, including IHCCA and EHCCA, is distinct from GBC in epidemiology, pathobiology, clinical presentation, and management[3]. Also, various studies have shown that IHCCA and EHCCA share different genetic backgrounds, risk factors, and clinical presentations[4].

According to epidemiological studies, the incidence rate of BTC is 0.35–2 cases per 100,000 annually in Western countries. However, the incidence rate is 40 times higher in Eastern regions than in Western countries. An abnormally high incidence rate (> 6 per inhabitants/yr) occurs in East Asian countries, such as South Korea, China, and Thailand, than in other regions[5-15]. One of the reasons for this higher incidence rate is an infection by parasites, such as *Opisthorchis viverrini* and *Clonorchis sinensis*, from consuming raw and undercooked fish[16]. Liver fluke infection is one of the risk factors associated with BTC[17-19]. The age-standardized incidence rate (ASR) of BTC showed geographical region specificity. The highest value (85 per 100,000 inhabitants/yr) was reported in Northeastern Thailand. However, 0.4 per 100,000 inhabitants/yr was reported in Canada[10]. Also, the incidence of GBC was the highest in Chile, followed

by Northern India, Poland, Southern Pakistan, Japan, and Israel[20]. An increased incidence of BTC (0.3–6 per 100,000 inhabitants/yr) and mortality (1–6 per 100,000 inhabitants/yr) indicated important global health problems. Moreover, the global trend in mortality from BTC increased from 2010-2014. The statistics suggested that BTC is a geographically region-specific disease with a globally increased incidence rate.

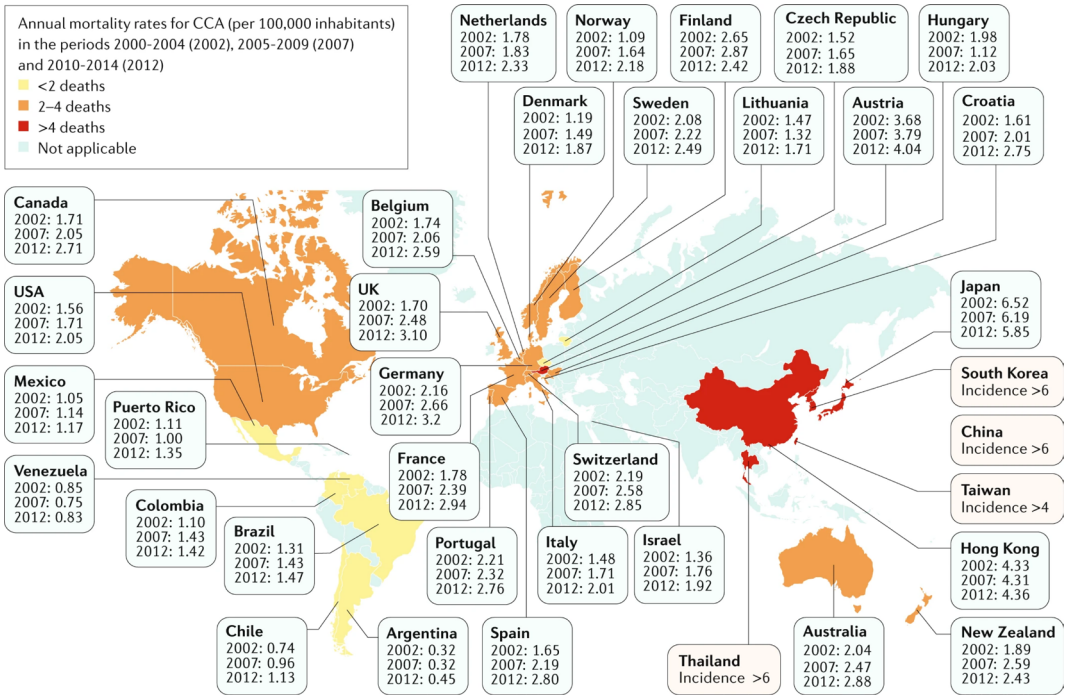

Figure 1. The mortality of biliary tract cancer[21].

BTC patients showed a low survival rate and poor prognosis. An assessment of the global BTC incidence was conducted in 22 countries and the incidence of BTC was second-werehighest in South Korea (10.37 per 100,000 inhabitants/yr)[22]. In a global multicenter study, among a total of 563 BTC patients with curative-intent hepatic resection, 400 (71.0 %) patients had a recurrence. The 5-yr survival rate of the recurrence patients was 23.6 % (median disease-free survival of 11.2 mo)[15]. In another international study, 306 BTC patients showed a recurrence rate of 58 % (n = 177)[12]. The 1, 3, and 5-yr survival rates were 71.2–82.8 %, 48.0–65.5 %, and 31.6–65.1 %, respectively, in a meta-analysis study of liver transplantation patients for unresectable perihilar cholangiocarcinoma (n = 438). This study showed a 51.7 % recurrence rate after 3 yrs of transplantation[14]. In South Korea, one of the countries with the highest BTC incidences, the 2018 annual report of the Korea Central Cancer Registry (KCCR) announced the 5-yr survival rate was 28.8 % in BTC patients. The 5-yr survival rate of BTC was also the lowest among nine major cancer types, including thyroid cancer (100 %), prostate cancer (94.4 %), breast cancer (93.3 %), renal cancer (84.1 %), stomach cancer (77.0 %), colorectal cancer (74.3 %), liver cancer (37.0 %), and lung cancer (32.4 %) in the KCCR report.

Clinical presentations of BTC are well established. Abdominal pain from neural compromise is one of the most common symptoms. Jaundice, fever, and weight loss were also reported by BTC patients. Additionally, thrombosis, thrombophlebitis, mental disturbances, and skin manifestations were observed in patients with BTC[23]. Although these symptoms are well known, BTC is difficult to diagnose in the early stages because it is usually asymptomatic.

A combination of Gemcitabine and Cisplatin, which is approved by the United States Food and Drug Administration (U.S. FDA), is one of the most common therapies used in baseline chemotherapy for unresectable BTC patients. Although this combination is the current gold standard for cancer, it showed a low median survival rate (11.7 mo) in the ABC-02 clinical trial[24]. In 2020, the U.S. FDA approved Pemigatinib, which is an inhibitor of *FGFR2* fusion or other rearrangements, as the first targeted therapy for advanced cholangiocarcinoma. *FGFR2* fusion has been reported in 9 to 14 % of patients with BTC, and Pemigatinib worked well for the

alteration in the FIGHT-202 trial. In 107 patients who received the Pemigatinib treatment in the clinical trial, 36 % of the overall response rate, 2.8 % of a complete response, and 33 % of a partial response were reported by the study[25]. The *FGFR1-4* inhibitor, Futibatinib, was tested in phase 2 of FOENIX-CCA2, an open-label clinical trial. One hundred three patients with advanced BTC were enrolled in this study, and treatment with Futibatinib in patients with IHCCA demonstrated its safety and effectiveness. The overall response rate was 34.3 % and the responses were all partial responses (n = 23). The median response time was 1.6 mo (1.0–4.9 mo) and the response duration was 6.2 mo (2.1–14.2 mo)[26]. Infigratinib is an *FGFR1-3* kinase inhibitor, which is one of the effective anti-cancer drugs for advanced BTC with *FGFR2* alterations. In the PROOF 301 clinical trial, 300 patients with advanced BTC were treated with oral Infigratinib and Gemcitabine plus Cisplatin (GemCis) to compare the drug efficacy in the two groups[27]. In a phase 2 study of Infigratinib, an overall response rate of 23.1 % (1 complete response and 24 partial responses) was reported[28]. Ivosidenib, a targeted *IDH1* small-molecule inhibitor approved by the U.S. FDA in 2021, was assessed for its efficacy and safety in advanced *IDH1*-mutant BTC in phase 3 of the ClarIDHy clinical trial. In this study, 185 patients were assigned to oral Ivosidenib (n = 124) or placebo (n = 61) daily in continuous 28-day cycles. Improved progression-free survival at 6 mo (32 %) and 12 mo (22 %) was shown in a group of patients receiving Ivosidenib compared with the placebo (no patients were free for the same timepoints)[29]. Also, an evaluation of Pembrolizumab plus Lenvatinib is ongoing in the LEAP-005 clinical trial[30].

There are several techniques for the diagnosis of BTC. Serum markers of malignancy are used for the detection of advanced-stage cancer. Carbohydrate antigen 19-9 and carbohydrate antigen 125 are also widely used for diagnosis. However, these markers have limitations because of their low specificity and sensitivity[31-34]. Imaging techniques, such as ultrasonography, contrast-enhanced ultrasonography (CEUS), computed tomography (CT), and magnetic resonance imaging (MRI), are also useful for BTC diagnosis and response assessment. Cholangiography, including magnetic resonance cholangiopancreatography (MRCP), endoscopic retrograde cholangiopancreatography (ERCP), and percutaneous transhepatic cholangiography

(PTC), have shown a powerful performance. Moreover, ERCP and MRCP showed high sensitivity (80–96 %), specificity (75–85 %), and accuracy (78–91 %)[35]. While these imaging tools are for diagnosis and staging, BTC-specific radiographic patterns do not exist[36]. Cytology from tissue biopsy (brush or fine needle) is a current standard method for cancer diagnosis. However, there are several challenges. It is a highly invasive technique where adequate amounts of the tumor cannot be retrieved for multiple tests. In particular, repeated sampling is not practical or ethical in stage IV cancer patients[37]. Tissue biopsy is limited to representing tumor heterogeneity and it cannot be used to monitor real-time drug response. To our knowledge, liquid biopsy is the best way to monitor the real time response to therapy in cancer patients. Liquid biopsy is a minimally invasive technique and monitors continuous tumor evolutions. It is also easy to repeatedly acquire adequate samples and represent tumor heterogeneity. However, optimized protocols are needed for the preparation of blood samples because of the short half-life of nucleic acids in plasma[38-41].

Liquid biopsy is defined as sample collection from various body fluids, including blood, urine, pleural fluid, and cerebrospinal fluid (CSF). Blood contains many biomarkers, such as circulating-cancer cells (CTCs), exosomes, and fragmented DNA (called 'cell-free DNA'). Generally, cell-free DNA (cfDNA) is mixed with DNA from normal cells and tumor cells. Among them, tumor-specific DNA from circulating-tumor cells is called circulating-tumor DNA (ctDNA). cfDNA, including ctDNA, is a main targetable marker in liquid biopsy[42]. cfDNA is released from cells into the circulatory system in the human body via two main contenders, which are cellular breakdown mechanisms and active DNA release mechanisms. The first mechanism involves necrosis, apoptosis, and mitotic catastrophe. Cell death caused by various factors, such as injury, surgery, and phagocytosis, in induced to release DNA strands outside of dead cells. Another mechanism occurs in living cells where differentiating cells release cfDNA, which is packaged inside exosomes or in other forms into the blood stream[43-45]. cfDNA has some biological features. For example, the size profile of cfDNA showed a nucleosome-dependent pattern. Mono-nucleosomal DNA (~168 bp), di-nucleosomal DNA (~343 bp), and tri-nucleosomal DNA (~533 bp) fragments were observed in blood plasma[46]. These fragmented DNAs are usually released from

dead cells by apoptosis, and among them, mono-nucleosomal DNA fragments are a major proportion of the total cfDNA in plasma. This short length cfDNA is an advantage for DNA sequencing because genomic DNA (gDNA) requires cutting into a suitable size range for DNA library construction. In certain health conditions, a very low concentration of cfDNA was observed, but cancer patients have a higher concentration of cfDNA than healthy individuals. For example, in a cancer study, the median level of cfDNA was 1.81 ng/mL in the healthy control group, while the cancer patient group showed a higher concentration (median 4.6 ng/mL)[47]. However, several researchers have suggested that the cfDNA concentration level is not suitable as a prognostic marker. In large sample sizes (n = 164, 218, and 268), changes in the cfDNA concentration were observed, but these changes were independent of clinical prognosis[48-50]. On the other hand, cfDNA is valuable in epigenetic studies. Hypermethylation of the *RASSF1A* promoter region in cfDNA is correlated with the size of the tumor mass in hepatocellular carcinoma cases. Also, the patients with hypermethylated *RASSF1A* at diagnosis or 1 yr after resection of the tumor showed poorer disease-free survival[51]. Many other studies reported that methylation of cfDNA is a useful epigenetic marker for studying cancer[51-57].

Due to the aforementioned advantages of cfDNA for cancer diagnosis and monitoring, a study using cfDNA with next-generation sequencing (NGS) is promising. Zill OA *et al*. studied cfDNA NGS with 26 BTC patients and a 54-gene panel[58], and Rothwell DG *et al*. investigated two BTC patients of a 100-pan-cancer cohort with a 641-gene panel[59]. Ettrich *et al*. studied 32 patients with a 15-gene panel and 8 patients with a 710-gene panel[60]. Okamura *et al*. described the results of 71 BTC patients among a 121-pan-cancer cohort using a 68–73-gene panel[61]. Although these studies showed remarkable cfDNA NGS results, there is not much BTC research because of the low BTC incidence in the West. Also, most studies concerning BTC using cfDNA NGS showed few samples and/or small gene panels. Despite the high incidence of BTC in South Korea, no study on BTC with cfDNA analysis exists to our knowledge.

BTC is an aggressive cancer with a poor prognosis. Sixty to seventy percent of patients with BTC were diagnosed at an advanced stage because early-stage BTC does not cause symptoms. Although the interest of targeted therapies has grown over the

past decades, only a few target drugs for BTC patients have been approved by the U.S. FDA (Pemigatinib and Ivosidenib). Many clinical trials have reported meaningful improvement using targeted therapies in patients with BTC, but better improvement is still required. cfDNA NGS is the best option for BTC diagnosis and monitoring. However, the number of studies using BTC with large sample sizes and gene panels is not sufficient in Western and Eastern countries.

In this prospective study, unresectable BTC patients (n = 41) were enrolled,ri and plasma samples (n = 137) were collected at multiple timepoints according to the chemotherapy process (pre-1st treatment; C1D1, pre-2nd treatment; C2D1, pre-4th treatment; C4D1, and progression disease; PD) from the patients for targeted sequencing of ctDNA with a large pan-cancer gene panel. We suggested candidates of actionable target genes and the potential roles of ctDNA NGS for drug response monitoring and prognosis in BTC patients.

II. MATERIALS AND METHODS

1. Study samples

Forty-one unresectable biliary tract cancer patients (n = 41) undergoing a palliative chemotherapy treatment at the Severance Hospital (Seoul, South Korea) were selected for this study (Table 1). We collected 18 mL of blood samples with DxTube^{TM}-cfDNA (Dxome, Seongnam-si, South Korea) containing preservation solutions at four timepoints which are pre-1st chemotherapy, pre-2nd chemotherapy, pre-4th chemotherapy, and progression disease. For removal of germline variants, patients' oral epithelial cells were collected by Oracollect·DNA (DNA Genotek, Ottawa, QC, Canada). According to RECIST 1.1 guideline, we defined the patients' clinical features such as best response rate[62]. Informed consent for all samples in this research was obtained for every participant and the study was approved by the institutional review board (IRB 4-2020-0083).

Table 1. Clinical characteristics of enrolled patients (n = 41)

Characteristics	*n*
Age (yr)	
Mean ± SD	62.85±11.17
Median	65
Range	41-84
Disease status	
Metastatic/unresectable	32
Recurrent	9
Sex	
Male	26
Female	15
Stage	
I	2
II	6
III	1
IV	32
Cancer type	
Intrahepatic cholangiocarcinoma; IHCCA	24
Gallbladder carcinoma; GBC	13
Extrahepatic cholangiocarcinoma; EHCCA	3
Ampulla of vater cancer; AoV	1
Histology	
Adenocarcinoma	38
Well differentiated	1
Moderately differentiated	20
Poorly differentiated	17
Sarcomatoid carcinoma	3
Response rate (best response)	
Complete response; CR	1
Partial response; PR	9
Stable disease; SD	23
Progressive disease; PD	6
Not applicable; NA	2
Blood collection	

pre-1st chemotherapy; C1D1	41
pre-2nd chemotherapy; C2D1	39
pre-4th chemotherapy; C4D1	31
Progression disease (recurrence); PD	27
First-line chemotherapy regimen	
Gemcitabine/Cisplatin	10
Gemcitabine/Cisplatin/Abraxane	28
Gemcitabine/Cisplatin/Immune checkpoint inhibitor*	3
Treatment efficacy	
Median duration of treatment (range; mo)	5.1 (0.2-20.1)
Progression free survival (range; mo)	5.3 (1.4-23.1)
Overall survival (range; mo)	9.3 (1.8-24.6)
Objective response rate (%)	24.4%
Disease control rate (%)	80.5%

* Bintrafusp alpha, bifunctional fusion protein targeting TGF-β and PD-L1

2. Genomic DNA extraction

Genomic DNA (gDNA) was extracted using QIAamp Blood Mini Kit (QIAGEN, Hilden, NRW, Germany) according to the manufacturer's instruction. Briefly, the buccal swab tube was incubated at 56 ℃ in water bath for 90-120 min. All lysis solution was transferred from the buccal swab tube to a 1.5 mL microtube. 60 uL of QIAGEN proteinase K was added to the solution, and it was incubated at 56 ℃ for 10 min. 700-750 uL of absolute ethanol was added to the solution and mixed well. The half solution was transferred from a 1.5 mL microtube to QIAamp mini spin column, and the column was centrifugated at 8,000 rpm for 1 min. The residual solution was transferred to the column and centrifugated in the same condition. The spin column was washed using AW1 and AW2 solution at 15,000 rpm for 3 min. We eluted gDNA with 70 uL of AE buffer from the column. The gDNA concentration was measured with the Qubit ds DNA BR assay kit (Thermo Fisher Scientific, Waltham, MA, USA).

3. Circulating tumor DNA extraction

ctDNA was extracted using Magnetic Circulating DNA Maxi Reagent (Dxome) according to the manufacturer's instruction. Briefly, plasma was separated from whole blood by double spin protocol (1,900 × g for 15 min and 1,900 × g for 20 min). 4 mL of plasma, 6 mL of GHH buffer, 60 uL of magnetic bead, and 400 uL of proteinase K were mixed in a 50 mL conical bottom tube. The mixture was incubated at room temperature for 20 min. The tube was placed on a magnetic stand for 2 min to separate the bead, and the supernatant was removed from the tube. The mixture by 750 uL of GDF buffer was transferred from the 50 mL conical bottom tube to the new 1.5 mL microtube. The tube was placed on a magnetic separator, and the supernatant was removed. For washing, 750 uL of PWG buffer was added and vortexed for 15 sec. The supernatant was removed and repeated this wash step. Finally, 65 uL of elution buffer was added to the tube containing the bead, and the tube was incubated at 56 ℃ for 5 min. The tube was placed on a magnetic stand and all supernatant was transferred to a new 1.5 mL microtube. The ctDNA concentration and purity were measured with the Cell-free DNA ScreenTape Assay (Agilent Technologies, Santa Clara, CA, USA). We

selected highly purified ctDNA (≥ 85 %) for accurate analysis because of contamination from leukocyte-driven DNA fragments. All extracted DNA samples were stored at -70 ℃ until we use them.

4. TMB500 panel

Tumor mutation burden (TMB) has emerged as one of the powerful biomarkers for cancer patients with immunotherapy[63]. Although whole exome sequencing (WES) is the best way for TMB assay, WES is limited by high cost, turn-around time, and tissue availability for routine diagnosis. Targeted panel sequencing is a currently practical method in the clinical field. In general, a gene panel for TMB assay was required over 300 genes or 1.0 Megabase pair (Mbp) covered region. Currently published panels approved by U.S. FDA for TMB assay are MSK-IMPACT (MSKCC) and FoundationOne CDx (F1CDx)[64]. These panels each covered 468 (1.22 Mbp) and 324 (0.8 Mbp) pan-cancer genes. We designed a customized pan-cancer gene panel that covered coding exons of 531 genes (1.63 Mbp), called TMB500, for targeted panel sequencing. TMB500 panel enables microsatellite instability (MSI) and copy number alteration (CNA). The panel gene candidates were selected by specialists in medical oncology based on a review of literature, databases, and guidelines. Also, interesting promoter or intronic regions like *TERT* promoter were included. The validation and performance of TMB500 panel were described as a previous study[65]. Briefly, TMB500 panel has low limit of detection (LoD; 0.24 %) and 95 % sensitivity (95 % confidence interval: 0.22-0.26). The panel showed high precision and linearity (r^2 = 0.87) for all single nucleotide variants. TMB500 panel gene list was described in APPENDICE A.

5. Targeted sequencing

A. DNA fragmentation

For gDNA sample, a DNA library was prepared from 200 ng of gDNA. First, 200 ng of intact gDNA in 100 uL of distilled water was prepared in 0.65 mL Bioruptor® Microtubes. Bioruptor® Pico sonication device (Diagenode, Denville, NJ, USA) was set at 4 ℃ and, the tube containing gDNA was sonicated into 150-250 base pair (bp)

for 30 min with 30 sec on/off. Fragmented DNA was mixed with 180 uL of AMPure XP beads (Beckman Coulter, Inc., Brea, CA, USA) and incubated at room temperature (RT) for 5 min. The tube was placed on magnetic stand for 1 min and, all supernatant was removed from the tube. The beads were washed with 500 uL of 80 % ethanol twice, then let them air-dry for 3 min. 37 uL of distilled water was added and incubated at RT for 5 min. The tube was placed into a magnetic stand for 3 min and 35 uL of supernatant was transferred to a new 1.5 mL microtube. To check the sheared DNA size distribution and concentration, 1 uL of fragmented DNA was run with 3 uL of D1000 TapeStation Reagent and ScreeTape on 4150 TapeStation System. Sheared DNA can be stored at -20 ℃ until needed. The fragmentation step was skipped in cfDNA because it was already fragmented at about 150 bp by apoptosis, necrosis, and various enzymatic reaction in the human body.

B. End repair and A-tailing

DNA library construction was performed using DxSeq™ Library Prep Reagent for Illumina (Dxome) with the manufacturer's instruction. Briefly, 100 ng of fragmented DNA or 15-30 ng of cfDNA in 35 uL of distilled water was added into a 0.2 mL PCR tube with 5 uL of 10× EA Buffer and 10 uL of EA Enzyme. Thermocycler condition for end repair and A-tailing was the following: 4 ℃ for 1 min, 20 ℃ for 30 min, 65 ℃ for 30 min, and held at 4 ℃ with heated lid at 75 ℃.

C. Adaptor ligation

The product from the above step was mixed with 20 uL of 5× Ligation Buffer, 5 uL of Adaptor, 10 uL of Ligation Enzyme, and 15 uL of nuclease-free water. The mixture was incubated at 20 ℃ for 15 min with the lid off and, 3 uL of USER enzyme was added to the tube containing the mixture. The tube was incubated at 37 ℃ for 15 min with a heated lid at 50 ℃. Adaptor ligated DNA was mixed with 100 uL of AMPure XP beads and incubated at room temperature (RT) for 5 min. The tube was placed on magnetic stand for 1 min and, all supernatant was removed from the tube. The beads were washed with 500 uL of 80 % ethanol twice, then let them air-dry for 3 min. Twenty-two microliter of distilled water was added and incubated at RT for 5 min.

The tube was placed into a magnetic stand for 3 min and 20 uL of supernatant was transferred to a new 1.5 mL microtube.

D. Pre-PCR

Twenty microliter of adaptor-ligated library, 5 uL of UDI, and 2× PCR Master Mix were mixed well in the tube. Thermocycler condition for pre-PCR was the following: 98 ℃ for 2 min, 10 or 14 cycles of 98 ℃ for 20 sec, 65 ℃ for 30 sec, and 72 ℃ for 1 min, then 72 ℃ for 10 min with a heated lid at 105 ℃. For removal of primer dimer and other reagents, 50 uL of AMPure XP bead was added into the tube and incubated at RT for 5 min. The tube was placed on magnetic stand for 1 min and, all supernatant was removed from the tube. The beads were washed with 500 uL of 80 % ethanol twice, then let them air-dry for 3 min. Thirty-two microliter of distilled water was added and incubated at RT for 5 min. The tube was placed into a magnetic stand for 3 min and 30 uL of supernatant was transferred to a new 1.5 mL microtube. To confirm the size and amplification of the DNA library, 1 uL of adaptor-ligated DNA was run with 3 uL of D1000 TapeStation Reagent and ScreenTape on 4150 TapeStation System (Agilent Technologies).

E. Hybridization capture-based target enrichment

The hybridization capture step was started with 8 libraries pooling in a tube. Briefly, 187.5 ng of each library was added in the same 1.5 mL microtube as one hybridization reaction. Pooled libraries in the tube were dried using HyperVAC VC2200 and HyperCOOLTM Freeze Dryer and Cooling Trap (Gyrozen, Gimpo-si, South Korea) at low heat conditions (37 ℃) for 2 hr.

All reagents for hybridization should be thawed on ice. Hybridization Mix per one reaction was incubated at 65 ℃ for 10 min and let cool down at RT for 5 min. In the new 0.2 mL PCR tube, 20 uL of the Hybridization Mix, 4 uL of TMB500 Probe Mix, and 3 uL of nuclease-free water were mixed and, the mixture was incubated at 95 ℃ for 2 min with a heated lid at 105 ℃. The mixture was immediately removed from the thermocycler and incubated for 5 min on ice. Five microliter of Blocker Solution and 8 uL of Universal Blockers were added to the tube containing the dried library pool

and mixed well by pipette. The library tube was incubated at 95 ℃ for 5 min with a heated lid at 105 ℃ and cooled down at RT for 3 min. All hybridization mixture with 30 uL of Hybridization enhancer was transferred into the library tube. The hybridization tube was incubated at 70 ℃ for 16 hr with a heated lid at 85 ℃.

For bead-based enrichment PCR, reagents were prepared before starting. Eight hundred microliter of Binding Buffer and 200 uL of Wash Buffer I was prepared at RT and, 700 uL of Wash Buffer II was preheated at 48 ℃. Streptavidin bead was incubated at RT for at least 30 min. In a 1.5 mL of microtube, 100 uL of streptavidin bead and 200 uL of Binding Buffer were added and vortexed. The tube was placed on the magnetic stand for 1 min, and all supernatant was removed. This wash step was repeated twice. After the final wash, 200 uL of Binding Buffer was added and mixed well.

The hybridization mixture was immediately transferred to the streptavidin bead tube. The bead tube was placed in a rotator at RT for 30 min (15 rpm). For wash off-targets, the bead tube was placed into the magnetic stand for 1 min and the supernatant was removed. 200 uL of Washing Buffer was added and mixed in the tube. All supernatant was removed using the magnetic stand and, 200 uL of pre-warmed Wash Buffer II was put into the tube. The tube was incubated at 48 ℃ for 5 min and placed into the magnetic stand for the removal of the supernatant. The supernatant was removed and, the wash step using Wash Buffers was repeated twice. After the final wash, residual buffers were removed by pipette and 45 uL of nuclease-free water was added.

F. Post -PCR

All process was performed on ice. Twenty microliter of captured DNA, 5 uL of amplification Primers, and 25 uL of 2× Post-PCR Master Mix were mixed in a new PCR tube. The thermocycler condition for pre-PCR was following; 98 ℃ for 45 sec, 10 cycles of 98 ℃ for 15 sec, 60 ℃ for 30 sec, and 72 ℃ for 1 min, then 72 ℃ for 10 min with a heated lid at 105 ℃. Seventy-five microliter of AMPure XP beads were put into a capture DNA tube and incubated at RT for 5 min. The tube was placed on the magnetic stand for 1 min, and all supernatant was removed. The beads were washed with 500 uL of 80 % ethanol twice, then let them air-dry for 3 min. Twenty-two

microliter of distilled water was added and incubated at RT for 5 min. The tube was placed into a magnetic stand for 3 min and 20 uL of supernatant was transferred to a new 1.5 mL microtube. One microliter of DNA library run with 3 uL of D1000 TapeStation Reagent and ScreenTape on 4150 TapeStation System to confirm DNA library construction and size distribution. The final DNA library concentration was measured with the Qubit dsDNA BR assay kit.

G. Sequencing

All libraries were pooled to 2 nM. Pooled library was denatured by 0.2 N NaOH, and the 2 nM denatured library was diluted with 400 mM Tris-HCl, pH 8 buffer to 400 pM, and mixed with PhiX sequencing Control V3 (Illumina, Inc., San Diego, CA, USA) as a spike-in control. Paired-end sequencing with 2 × 150 bp was performed using the Novaseq 6000 system (Illumina, Inc.). We targeted at least 490 million reads and > 30,000 × average depth per cfDNA sample. The average depth of germline paired samples was > 3,000 ×.

6. Data processing and variant calling

Raw FASTQ files were mapped to the human reference genome of GRC37 (hg19) by Burrows-Wheeler alignment[66]. Single nucleotide variants (SNVs) and small indels were called using the PiSeq algorithm. ExomeDepth is calculated by an in-house pipeline for CNAs detection. Detected variants were annotated using the DxSeq software (Dxome). Called somatic variants were automatically classified using several guidelines such as the Association of Molecular Pathology (AMP), American Society of Clinical Oncology (ASCO), and College of American Pathologists (CAP), and the American College of Medical Genetics and Genomics (ACMG) and the AMP were used for germline variants[67, 68].

cfDNA requires optimized high-sensitivity techniques such as the molecular barcode. However, molecular barcodes often showed low performance due to index hopping errors. We used Positional index sequencing (PiSeq) algorithm (Dxome), which minimizes the hopping errors for cfDNA NGS.

7. Variant interpretation

Variants classified three types as pathogenic, likely pathogenic, or unknown significance according to the ACMG/AMP guidelines and/or tiers 1, 2, or 3 according to AMP/ASCO/CAP guidelines.

8. Assessment of concordance rate between tissue and cfDNA

We compared somatic alterations from NGS results for identifying the concordance rate between tumor tissue and cfDNA. Tissue NGS was performed with TruSight Oncology 500 panel (TSO500, Illumina) and primary tumor tissue at pre-1st chemotherapy. TSO500 panel contains similar pan-cancer genes to TMB500 panel (APPENDICE A). Briefly, 40 ng of gDNA from formalin-fixed paraffin-embedded tissues (FFPE) with high tumor cellularity (> 30 %) was used for DNA library, and it was captured and sequenced with TSO 500 panel. The concordance rate was calculated by the following formula:

$$\text{Concordance rate (\%)} = (X \div Y) \times 100$$

X = No. of nonsynonymous somatic variants from tissue and cfDNA NGS; Y = Total No. of nonsynonymous somatic variants from tissue NGS.

9. Estimation of microsatellite instability

Microsatellite instability (MSI) is one of the promising biomarkers in cancer study. It is caused by the error of the DNA mismatch repair (MMR) process. MSI-high (MSI-H) status means MMR-deficient status in cancer. It indicated that many neoantigens present in patients' bodies with cancer and the patients are sensitive to immunotherapy[69]. MSI associated studies have reported that MSI is a marker that predicts who can have benefits from immunotherapy[70-72]. Standard PCR for microsatellite markers in clinical labs recommends by National Cancer Institute (NCI) to use only five markers[73]. We assessed MSI status by targeted sequencing. The NGS for MSI can provide more markers than PCR. Many informative markers offer higher reliability and reproducibility in diagnosis. We defined that MSI-H showed mutations in 20 %.

10. Estimation of tumor mutation burden

Tumor mutation burden was estimated by the following formula:

Tumor Mutation Burden = A ÷ B

A = No. of nonsynonymous somatic mutations, B = 1.63 Mbp of TMB500 size

TMB level applied no threshold as a maker was not valuable. Zehir A *et al*. proposed a reasonable threshold as "median TMB + 2 × IQR (TMB)"[74]. We used a modified threshold (median TMB + 1.25 × IQR) by Fernandez EM *et al*. from the original threshold[75].

11. Pathway analysis

Gene set of tier 1-3 variants from TMB500 targeted panel sequencing was analyzed. The key pathways and genes were curated from literature and detected somatic mutations were categorized by them.

III. RESULTS

1. Sequencing quality

We ran sequencing in five batches. The mean depth of the batches was 47,061 ×. The mapping read rate was over 99.9 % to the human reference genome (hg19). The on-target rate was 65 % (Table 2).

Table 2. Sequencing run quality

No.	Total reads	Mapped reads	Mean insert size (bp)	Mean depth (x)	On target (%)
Batch1	1,143,790,342	1,142,893,253	216	67,261	66
Batch2	685,939,504	685,447,278	210	41,383	67
Batch3	755,648,425	755,085,774	206	45,179	66
Batch4	701,560,248	701,063,913	202	39,633	63
Batch5	731,781,435	731,172,979	206	41,850	64

2. High concordance rate between tissue NGS and cfDNA NGS

We compared variants between tissue NGS and cfDNA NGS to assess the concordance rate. A total of 41 gene mutations were detected from tissue NGS and cfDNA NGS (Figure 2). Forty-seven variants were observed in both NGS methods, and 29 variants were identified in the single method (tissue: 8 and cfDNA: 21). According to the formula in the *Materials and Methods* section, we generated a high concordance rate (85.19 %). Although a few variants were discordant, the most clinically significant variants were concordant.

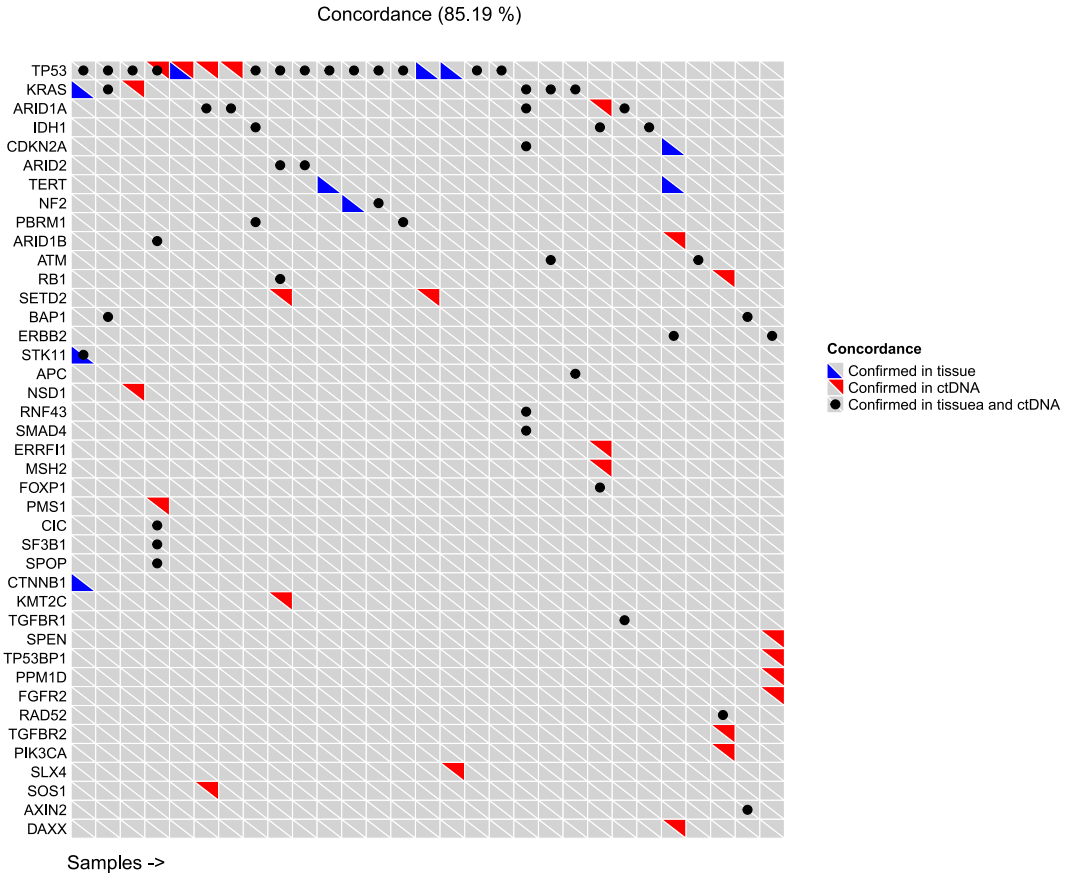

Figure 2. Concordance between tissue NGS and cfDNA NGS.

Concordance plot showing shared genes in both or each single NGS. Detected genes were annotated at the left side. Each column indicates individual patients. The blue and red triangle indicate a mutated gene confirmed in tissue NGS or cfDNA NGS. The black dot shows the mutated gene confirmed in both.

3. Spectrum of cfDNA somatic variants in biliary tract cancer

We sequenced the cfDNA of BTC patients with 531 pan-cancer genes. Overall, after filtering out no significant variants, clonal hematopoiesis of indeterminate potential (CHIP), and germline variants, we identified 408 mutated genes from cfDNA NGS. Clinical information, including age, gender, cancer type, response rate (RR), and progression-free survival (PFS), was annotated on the bottom side. Pre-1st chemotherapy and progression disease results are presented in Figures 3 and 4.

TP53 (59 %), *ARID2* (22 %), *KRAS* (17 %), *ARID1A* (15 %), *ARID1B* (15 %), *PDE4DIP* (15 %), *CHD4* (12 %), *FAT1* (12 %), *FGFR2* (12 %), *IDH1* (12 %), *PIK3CA* (12 %), *PTCH1* (12 %), *SPEN* (12 %), *APC* (10 %), *ATM* (10 %), *ATR* (10 %), *ERBB4* (10 %), *KAT6A* (10 %), *NOTCH1* (10 %), and *SPOP* (10 %) mutations showed high frequencies in the pre-1st chemotherapy timepoint (Figure 3). *TP53* (61 %), *ARID2* (39 %), *PTPRT* (39 %), *ATM* (28 %), *EGFR* (22 %), *KMT2A* (22 %), *KRAS* (22 %), *POLD1* (22 %), *PREX2* (22 %), *SPEN* (22 %), *BCL6* (17 %), *CHD4* (17 %), *KMT2C* (17 %), *MYH11* (17 %), *NEGR1* (17 %), *NUMA1* (17 %), *PDE4DIP* (17 %), *PIK3R1* (17 %), and *ZFHX3* (22 %) alterations were highly ranked in progression disease (Figure 4).

A total of 19 CNAs were observed at all timepoints. Among them, 11 duplications (*MYC*, *ERBB2*, *FGFR2*, *RAD54L*, *GATA4*, *ARID2*, *MDM2*, *PIK3R3*, *NRAS*, *CDK12*, and *EGFR*) and 3 deletions (*CDKN2A*/*B* and *IDH1*) were identified in pre-1st chemotherapy. Eight duplications (*MYC*, *ERBB2*, *FGFR2*, *GATA4*, *ARID2*, *MDM2*, *CDK12*, and *EGFR*) and the *CDKN2A* deletion were observed in progression disease (Figures 3 and 4). Among the detected CNAs, *RAD54L* (NM_003579.3; exon 10), *BCL2L11* (NM_138625.3; exon 3), and *PIK3R3* (NM_001303428.1; exon 1) were partially duplicated or deleted, and other CNAs were fully altered.

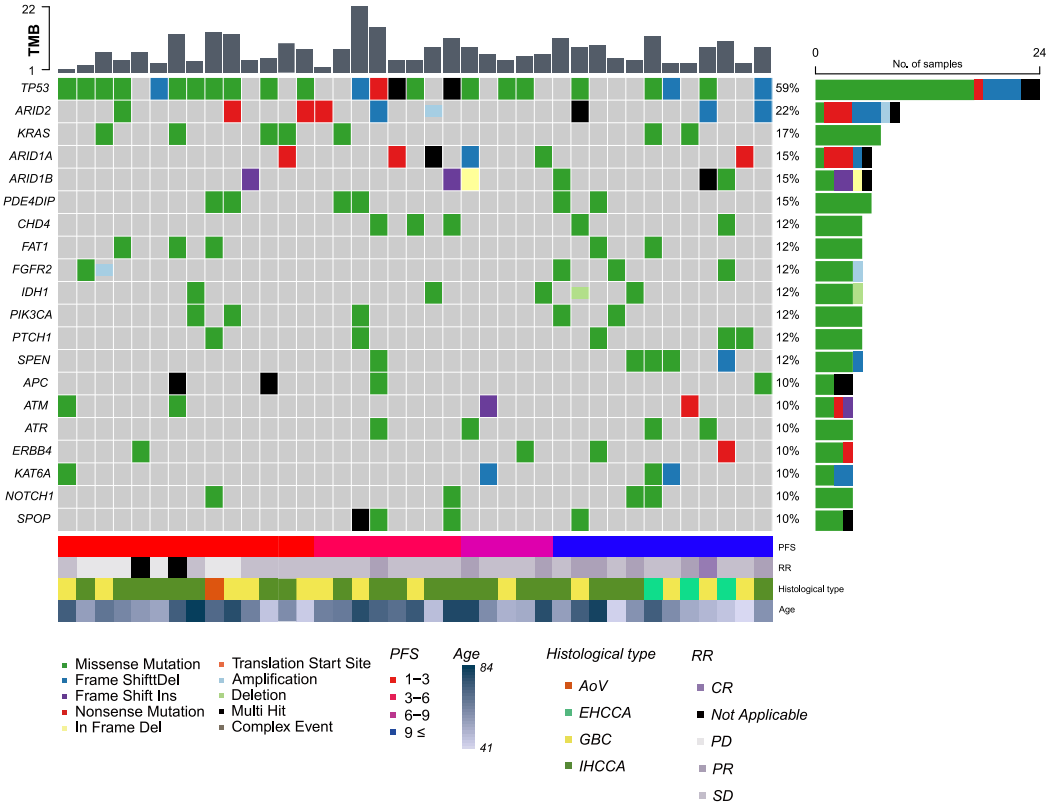

Figure 3. Top 20 mutational gene landscape of BTC patients in pre-1st chemotherapy.
The oncoplot showing the top mutated genes. The central plot indicates the type of mutation in each patient. The top bar graph shows the TMB value in each patient. Mutated gene symbols are on the left side and the frequency of the mutated genes are on the right side. The bottom annotations show the clinical features of the patients. PFS; progression-free survival, AoV; ampulla of vater cancer, EHCCA; extrahepatic cholangiocarcinoma, IHCCA; intrahepatic cholangiocarcinoma, GBC; gallbladder cancer, CR; complete response, PR; partial response, SD; stable disease, PD; progressive disease.

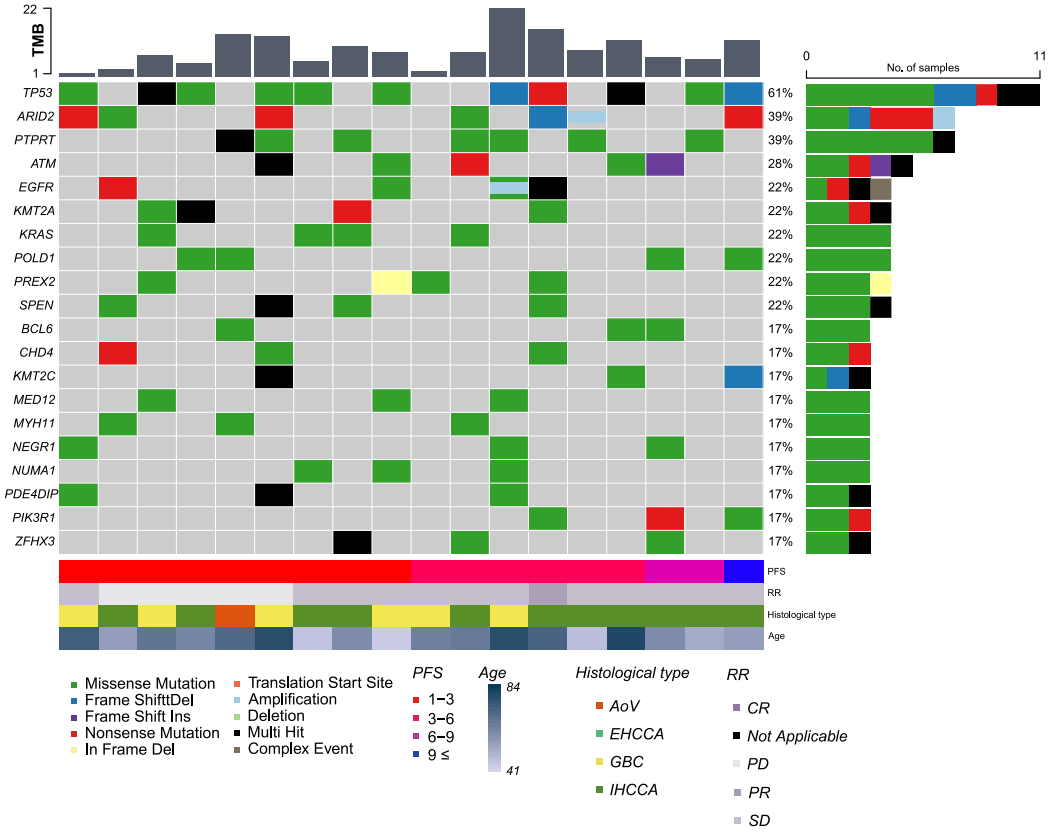

Figure 4. Top 20 mutational gene landscape of BTC patients in progression disease.

The oncoplot showing the top mutated genes. The central plot indicates the type of mutation in each patient. The top bar graph shows the TMB value in each patient. The mutated gene symbols are on the left side and the frequency of the mutated genes is on the right side. The bottom annotations show the clinical features of the patients. PFS; progression-free survival, AoV; ampulla of vater cancer, EHCCA; extrahepatic cholangiocarcinoma, IHCCA; intrahepatic cholangiocarcinoma, GBC; gallbladder cancer, CR; complete response, PR; partial response, SD; stable disease, PD; progressive disease.

4. Comparison of the number of patients with differentially mutated genes between timepoints

We compared mutational profiles throughout the chemotherapy process including progression disease. When we compared patients with mutated genes between the pre-1st chemotherapy, pre-2nd chemotherapy, and pre-4th chemotherapy timepoints, there were no significant changes (Figure 5A and B). When patients developed progression disease, the number of patients with the *PTPRT* mutation significantly increased (Figure 5C, $p = 0.005$). Also, the number of patients with the *PTPRT* mutation significantly increased when we compared the number of patients between pre-1st chemotherapy and progression disease (Figure 5D, $p = 0.0006$).

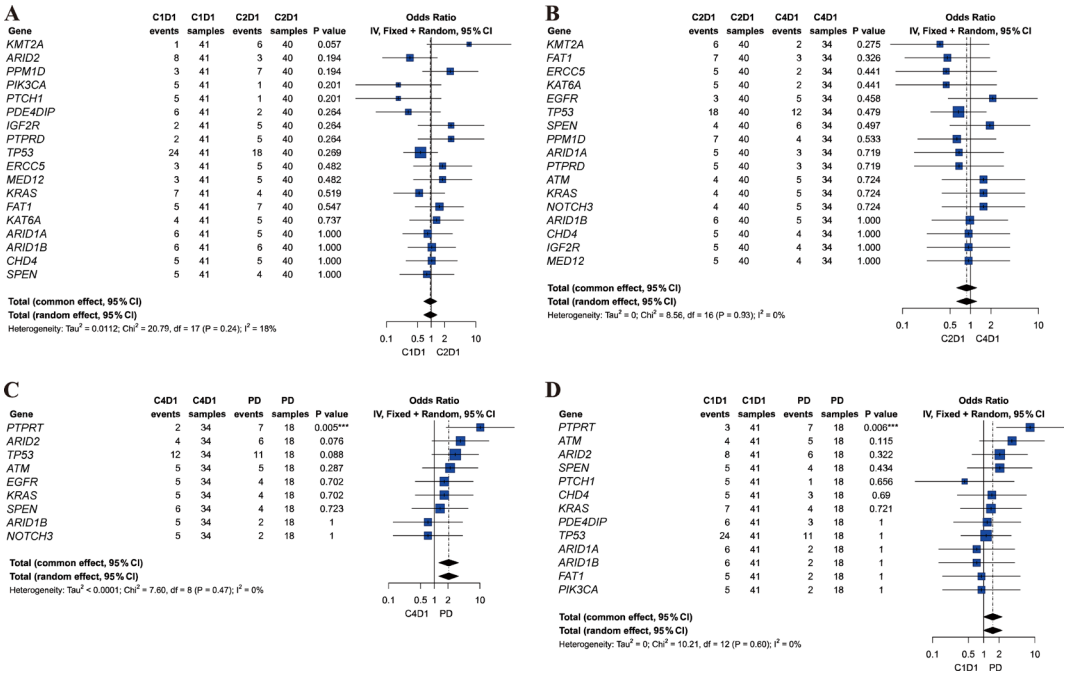

Figure 5. Comparison of the number of patients with mutated genes between multiple timepoints.

(A) The upper-left forest plot shows a comparison of the patients who have mutated genes between C1D1 and C2D1, and (B) the upper-right forest plot indicates a comparison of patients who have mutated genes between C2D1 and C4D1. (C) The lower-left forest plot shows a comparison of patients who have mutated genes between C4D1 and PD, and (D) the lower-right forest plot indicates patients who have mutated genes between C1D1 and PD. P values were calculated via Fisher's exact test. C1D1; pre-1st chemotherapy, C2D1; pre-2nd chemotherapy, C4D1; pre-4th chemotherapy, PD; progression diseases, OR; odd ratio, NS; not significant.

5. Enrichment pathway of significant variants

We analyzed the enrichment pathway of mutated genes. Identified mutated genes were categorized into several key pathways of BTC. 'Epigenetic regulation,' 'TP53 signaling,' 'RAS/RAF/ERK pathway,' 'PI3K/AKT/mTOR pathway,' 'DNA damage and instability,' 'DNA repair,' 'Cell cycle,' 'Angiogenesis,' 'NOTCH signaling,' 'Wnt signaling,' 'Cell death,' 'ERBB signaling,' 'Hedgehog pathway,' 'Hippo signaling,' 'Immune response,' and 'TGF-β/SMAD signaling' were primarily observed in all timepoints. 'TP53 signaling,' 'Epigenetic regulation,' and 'RAS/RAF/ERK pathway' showed a high population at pre-1st chemotherapy and progression disease. The ranking of 'IL-6/STAT3 signaling' later rose remarkably (Figures 6 and 7).

In the statistical pathway analysis when we compared the number of patients who had mutated pathway genes between pre-1st chemotherapy, pre-2nd chemotherapy, and pre-4th chemotherapy, there were no significant changes (Figure 8A and B). When patients developed progression disease, the frequency of all pathways was increased. Among them, the 'PI3K/AKT/mTOR pathway,' 'TP53 signaling,' 'TGF-β/SMAD signaling,' 'Cell death,' and 'IL-6/STAT3 signaling' were significantly increased (Figure 8C). Also, 'IL-6/STAT3 signaling' was significantly increased when we compared the number of patients who had mutated pathway genes between pre-1st chemotherapy and progression disease (Figure 8D).

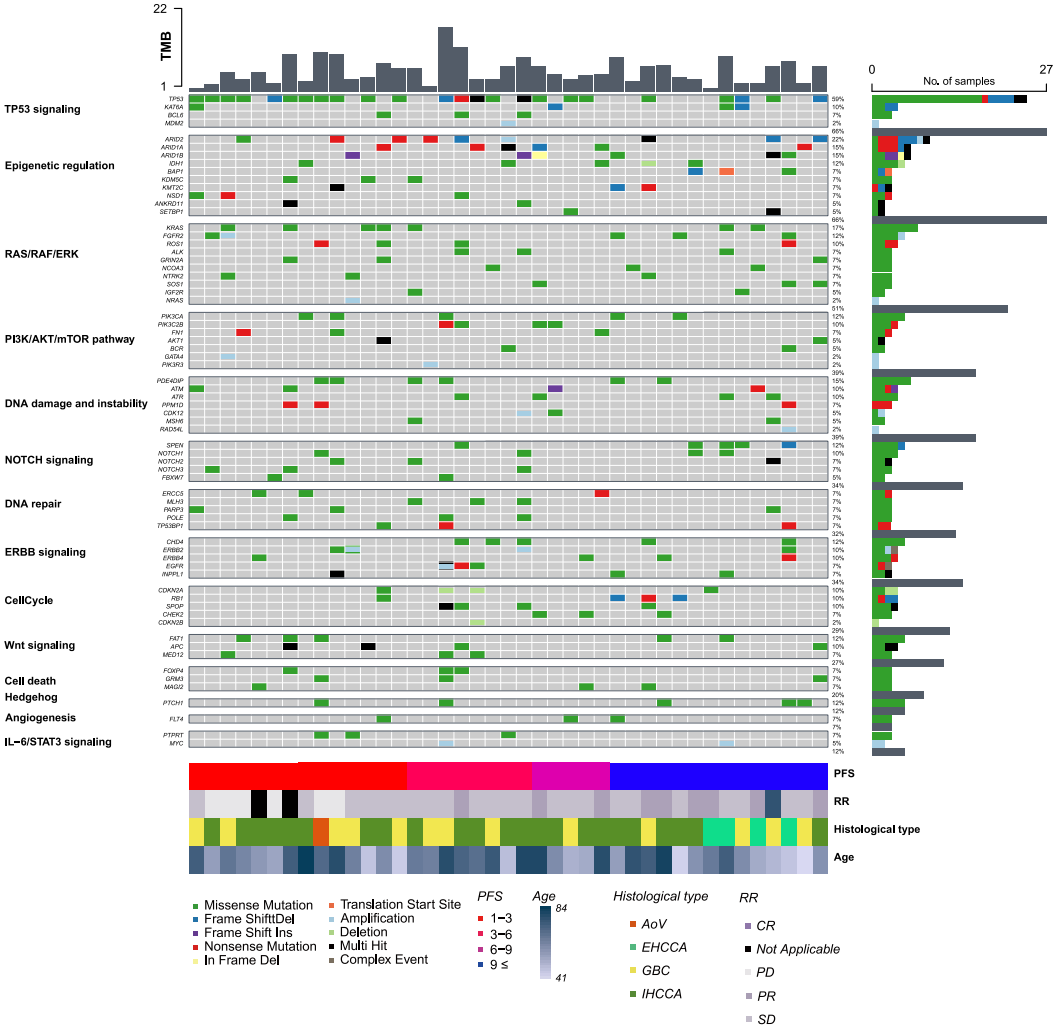

Figure 6. Top pathway enrichment of BTC patients in pre-1st chemotherapy.

The oncoplot showing the key pathway and genes. The central plot indicates the type of mutation in each patient. The top bar graph shows the TMB value in each patient. The left side annotation shows the mutated gene symbol and its pathway. The right-side annotation indicates the frequency of the mutated gene in the cohort. The bottom annotations show the clinical features of the patients. PFS; progression-free survival, AoV; ampulla of vater

cancer, EHCCA; extrahepatic cholangiocarcinoma, IHCCA; intrahepatic cholangiocarcinoma, GBC; gallbladder cancer, CR; complete response, PR; partial response, SD; stable disease, PD; progressive disease.

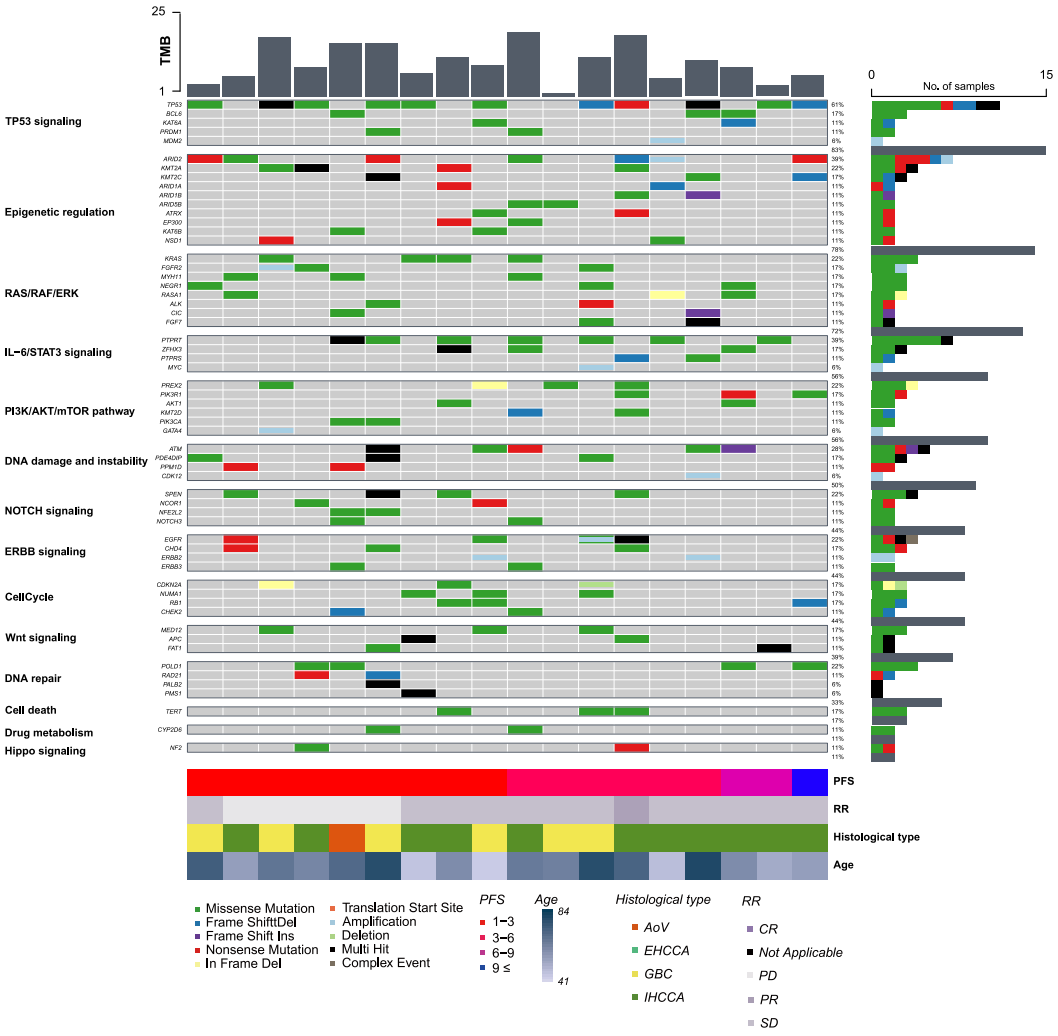

Figure 7. Top pathway enrichment of BTC patients in progression disease.

The oncoplot showing the key pathway and genes. The central plot indicates the type of mutation in each patient. The top bar graph shows the TMB value in each patient. The left side annotation shows the mutated gene symbol and its pathway. The right-side annotation indicates the frequency of the mutated gene in the cohort. The bottom annotations show the clinical features of the patients. PFS; progression-free survival, AoV; ampulla of vater

cancer, EHCCA; extrahepatic cholangiocarcinoma, IHCCA; intrahepatic cholangiocarcinoma, GBC; gallbladder cancer, CR; complete response, PR; partial response, SD; stable disease, PD; progressive disease.

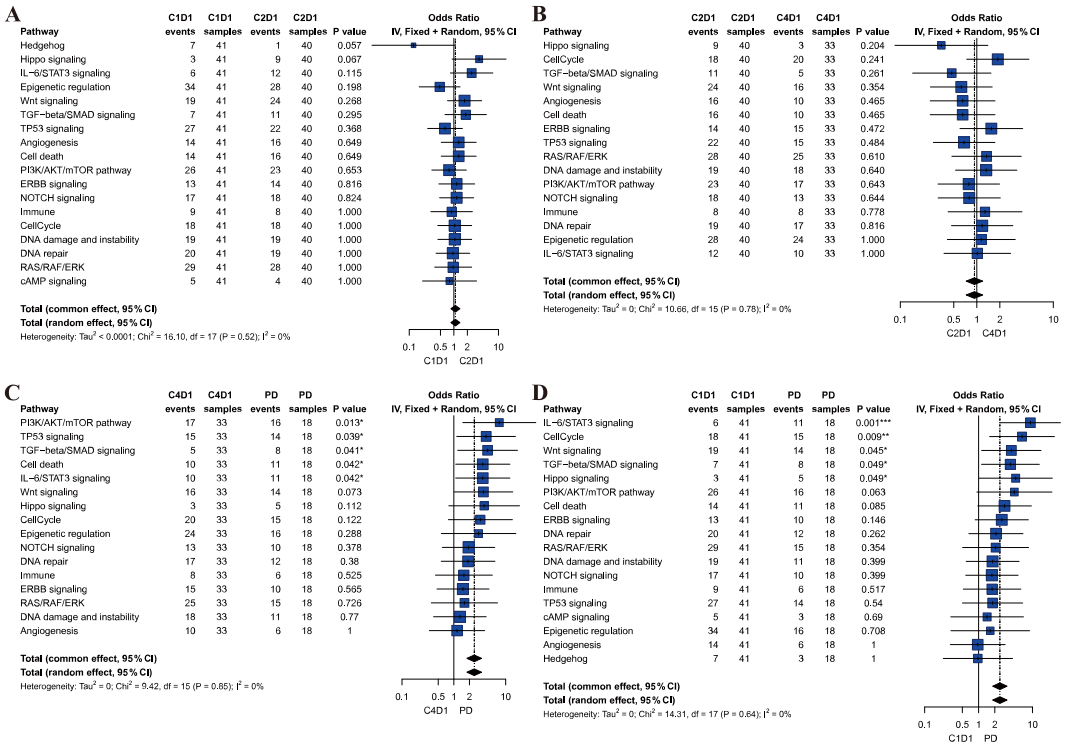

Figure 8. Comparison of the number of patients who had mutated pathway genes between multiple timepoints.

(A) The upper-left forest plot shows a comparison of patients who had mutated pathway genes between C1D1 and C2D1, and (B) the upper-right forest plot indicates a comparison of patients who had mutated pathway genes between C2D1 and C4D1. (C) The lower-left forest plot shows a comparison of patients who had mutated pathway genes between C4D1 and PD, and (D) the lower-right forest plot indicates patients who had mutated pathway genes between C1D1 and PD. P values were calculated via Fisher's exact test. C1D1; pre-1st chemotherapy, C2D1; pre-2nd chemotherapy, C4D1; pre-4th chemotherapy, PD; progression diseases, OR; odd ratio, NS; not significant.

6. The *PTPRT* gene contributes to poor prognosis of BTC patients

We observed the acquired variants (*PTPRT* E181K, *PTPRT* E468K, *PTPRT* P1079T, *PTPRT* A1096G, and *PTPRT* R1188C) of the PTPRT domains at progression disease (Figure 9).

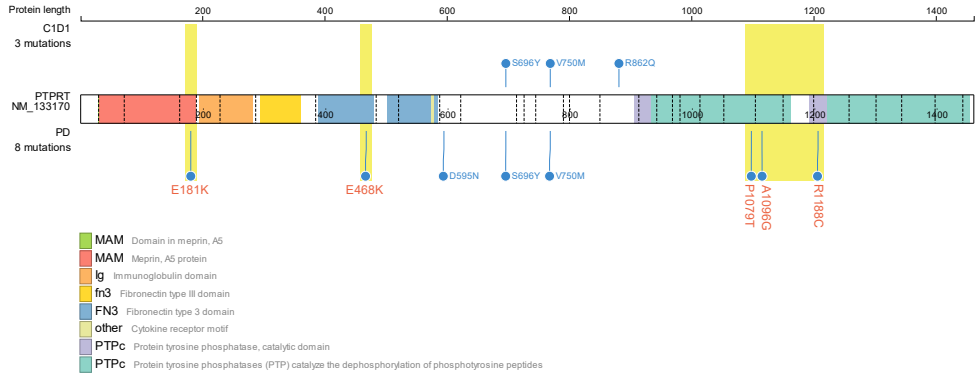

Figure 9. Baseline variants and acquired variants of *PTPRT*.

The lollipop plot shows the PTPRT protein structure and its mutations. The upside of the plot indicates variants at C1D1 while the downside of the plot indicates acquired variants at PD. The highlights show the acquired variants of the PTPRT domains. C1D1; pre-1st chemotherapy and PD; progression disease.

7. Platinum drug resistance genes affects prognosis of BTC patients

Our cohort was treated with GemCis as a first-line regimen. We divided the patients who had PDR variants at pre-1st chemotherapy into two groups: (1) patients with persistently platinum drug resistance (PDR) variants from pre-1st chemotherapy to pre-2nd chemotherapy (persistent PDR group; n = 27), and (2) patients without persistent PDR variants from pre-1st chemotherapy to pre-2nd chemotherapy (non-persistent PDR group; n = 10).

As shown in Figure 10A, the non-persistent PDR group showed prolonged PFS (p = 0.008). Also, we found that more long responders belonged to the non-persistent PDR group. We expanded this concept to pre-4th chemotherapy. First, we excluded patients without pre-4th chemotherapy samples (n = 4) and divided the groups into two in the same way (persistent PDR group; n = 24 and non-persistent PDR group; n = 9). We observed the same trend at pre-4th chemotherapy (p = 0.033) in Figure 10B. In addition, four long responders belonged to the non-persistent PDR group. The detected PDR genes are described in APPENDICE B.

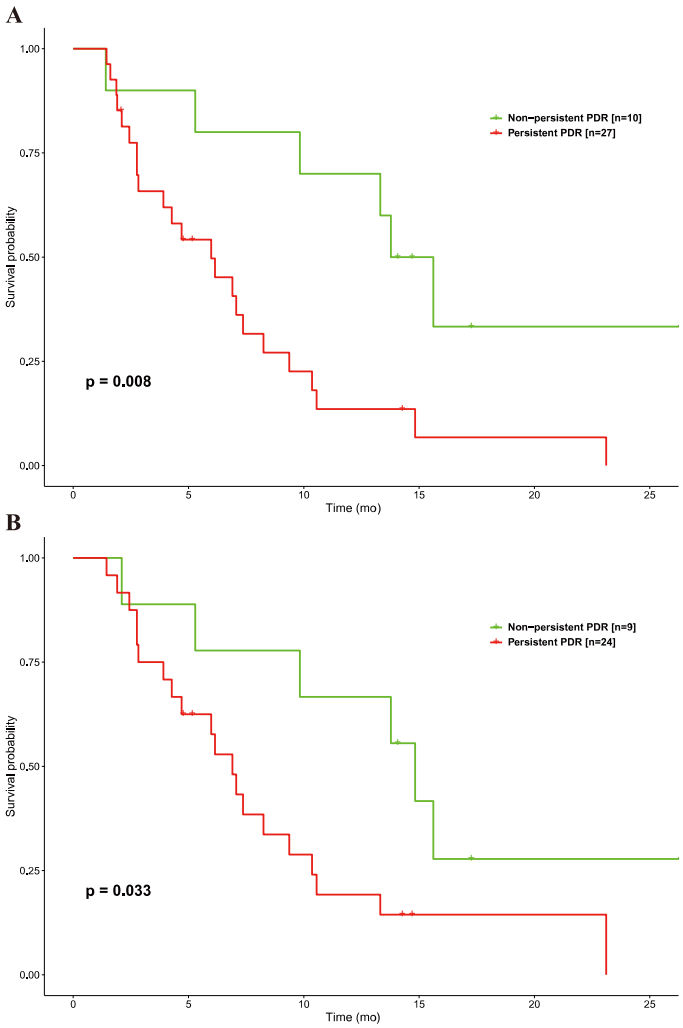

Figure 10. The Kaplan-Meier plot between PDR groups.

The PFS analysis of patients who had platinum drug resistance. (A) PFS was compared between the persistent PDR group and the non-persistent PDR group from pre-1st chemotherapy to pre-2nd chemotherapy. (B) PFS was compared between the persistent PDR group and the non-persistent PDR group from pre-1st chemotherapy to pre-4th chemotherapy. The red line indicates the persistent PDR group, and the green line indicates the non-persistent PDR group. PFS; progression-free survival, PDR; platinum drug resistance.

8. Change of pathway frequency in non-persistent PDR patients

To observe the pathway frequency change according to the PDR groups under chemotherapy, we enriched all mutations to curated pathways. Many pathways showed similar frequencies under chemotherapy. 'DNA repair,' 'ERBB pathway,' and 'Cell death' showed constantly low frequencies under chemotherapy, including pre-1st chemotherapy. 'TP53 signaling,' 'PI3K/AKT/mTOR pathway,' and 'IL-6/STAT3 pathway' showed a reduced frequency trend, although they were not significant. STAT3 pathway mutations were not detected at pre-2nd chemotherapy and pre-4th chemotherapy (Figure 11).

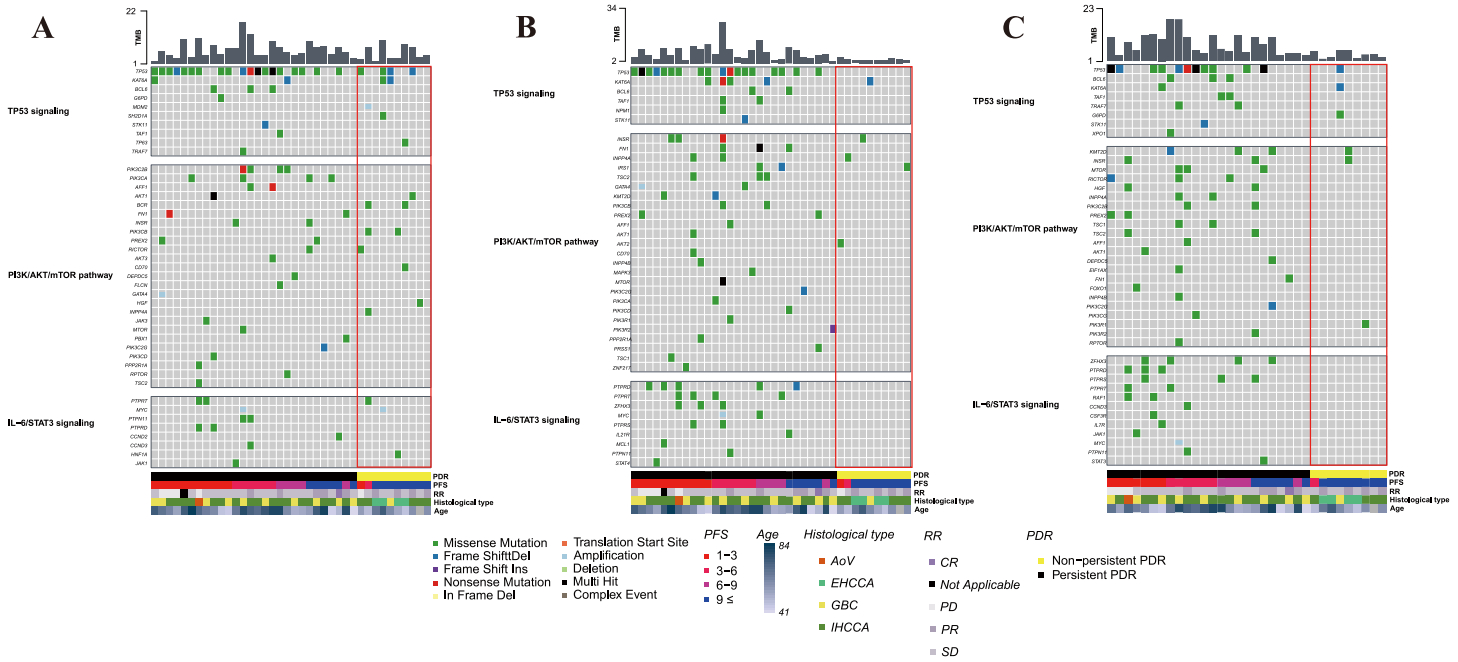

Figure 11. Comparison of pathway frequencies in patients with PDR variants under chemotherapy.

Comparison of the frequencies of the 'PI3K/AKT/mTOR pathway,' 'IL-6/STAT3 pathway,' and 'TP53 signaling' between (A) pre-1st chemotherapy, (B) pre-2nd chemotherapy, and (C) pre-4th chemotherapy. The bottom annotations indicate the clinical features of the patients. The red rectangles indicate the pathway mutations of the non-persistent PDR patients. PDR; platinum drug resistance.

9. PI3K and STAT3 pathways affect the prognosis of BTC patients

To analyze the effect of the 'PI3K/AKT/mTOR pathway' and 'IL-6/STAT3 pathway' mutations in BTC patients, we compared PFS between (1) patients who had PI3K-positive and STAT3-positive mutations under chemotherapy (n = 6), (2) patients who had PI3K-positive or STAT3-positive mutations under chemotherapy (n = 23), and (3) patients who had PI3K-negative and STAT3-negative mutations under chemotherapy (n = 12). The first group showed the lowest PFS, and the highest PFS was observed in the third group (Figure 12). The two groups showed significantly different PFS (p = 0.0074).

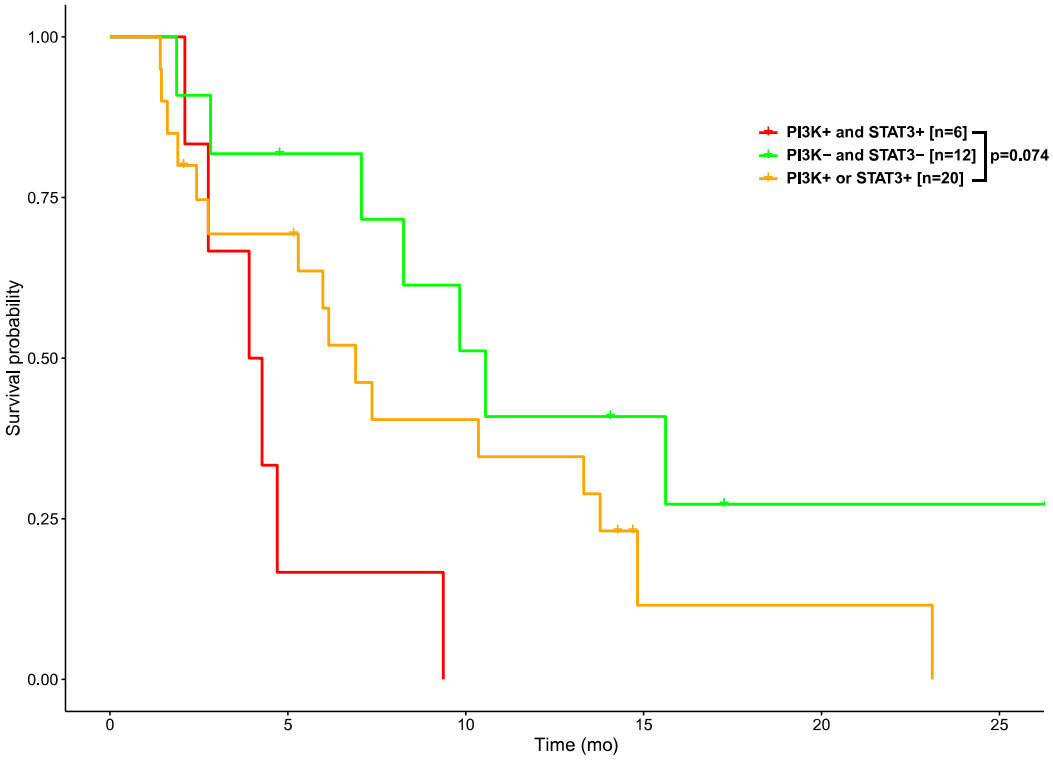

Figure 12. The Kaplan-Meier plot between the PI3K and STAT3 group.

Comparison of PFS between patients who had mutated 'PI3K/AKT/mTOR pathway' and 'IL-6/STAT3 pathway' genes. The red line indicates the PI3K-positive and STAT3-positive group. The yellow line indicates the PI3K-positive or STAT3-positive group. The green line indicates the PI3K-negative and STAT3-negative group. PFS; progression-free survival.

10. TMB is a potential prognostic marker

Based on the previous results, we assumed that a reduced TMB level affected the prognosis of patients with BTC under chemotherapy. We compared various TMB thresholds. First, we proposed three delta TMB (dTMB) thresholds: (1) 20 % increased dTMB / 20 % decreased dTMB, (2) 20 % increased dTMB / 30 % decreased dTMB, and (3) 30 % increased dTMB / 30 % decreased dTMB (Figure 13). At C1D1–C2D1, all thresholds showed a significantly different PFS between the decreased group and increased group (p = 0.0046, 0.0025, and 0.001, respectively). However, at C1D1–C4D1, only the 20 % increased dTMB / 30 % decreased dTMB and 30 % increased dTMB / 30 % decreased dTMB thresholds showed a significantly different PFS between the decreased group and the increased group (p = 0.024 and 0.031, respectively). There was no significance in the 20 % increased dTMB / 20 % decreased dTMB threshold (p = 0.094).

Second, we confirmed a significant difference in PFS (p = 0.0035) between the high TMB group (TMB-H) and the low TMB group (TMB-L) using the specific threshold at pre-1st chemotherapy (Figure 14A). Also, a prolonged survival rate was observed in the TMB-L group (p < 0.0001) in overall survival (Figure 14B).

Third, we combined the 20 % increased dTMB / 30 % decreased dTMB and TMB-L/H thresholds. The result of using this combined threshold corresponded with the expectation that decreased&TMB-L patients showed better PFS than increased&TMB-L patients. Specifically, decreased&TMB-L, stable&TMB-L, increased&TMB-L, stable&TMB-H, and increased&TMB-H groups were observed. The prognosis was better in order of mention at C1D1–C2D1 and C1D1–C4D. The decreased&TMB-L group showed more significantly prolonged PFS than the increased&TMB-L group (p = 0.00655), and patients in the stable&TMB-H group had poorer PFS than those in the stable&TMB-L group (p = 0.01) at C1D1–C2D1. We observed the same trend at C1D1–C4D1 (Figure 15A and B).

We analyzed the TMB levels at each timepoint using clinically prognostic parameters. First, we compared the TMB levels at each timepoint, and the progression disease group showed significantly increased TMB levels (Figure 16A). The TMB levels were compared with the complete response + partial response (CR+PR) and

stable disease + progressive disease (SD+PD) groups (Figure 16B). However, we did not observe any significant changes.

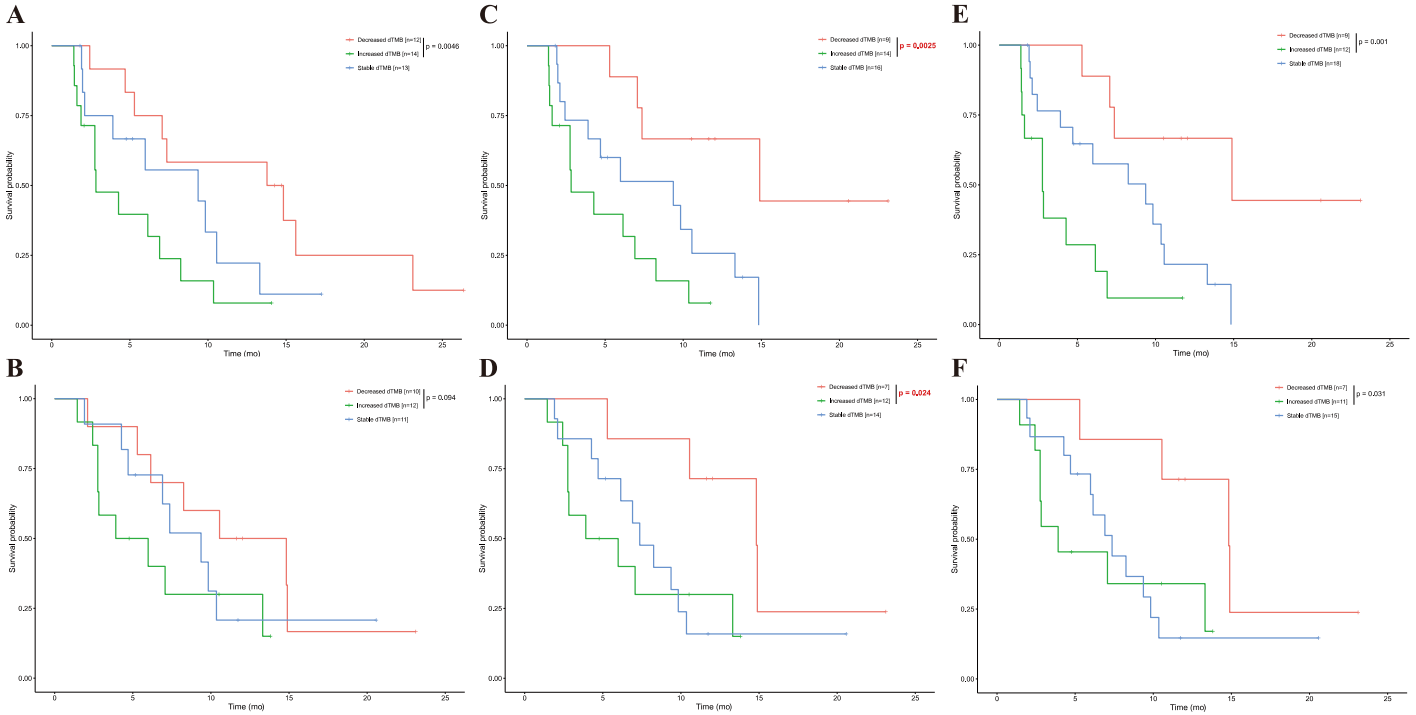

Figure 13. The Kaplan-Meier plot for dTMB thresholds.

The first threshold (20 % increased dTMB / 20 % decreased dTMB) was applied at (A) C1D1–C2D1 and (B) C1D1–C4D1. The second threshold (20 % increased dTMB / 30 % decreased dTMB) was applied at (C) C1D1–C2D1 and (D) C1D1–C4D1. The third threshold (30 % increased dTMB / 30 % decreased dTMB) was applied at (E) C1D1–C2D1 and (F) C1D1–C4D1. C1D1; pre-1st chemotherapy, C2D1; pre-2nd chemotherapy, C4D1; pre-4th chemotherapy, dTMB; delta tumor mutation burden.

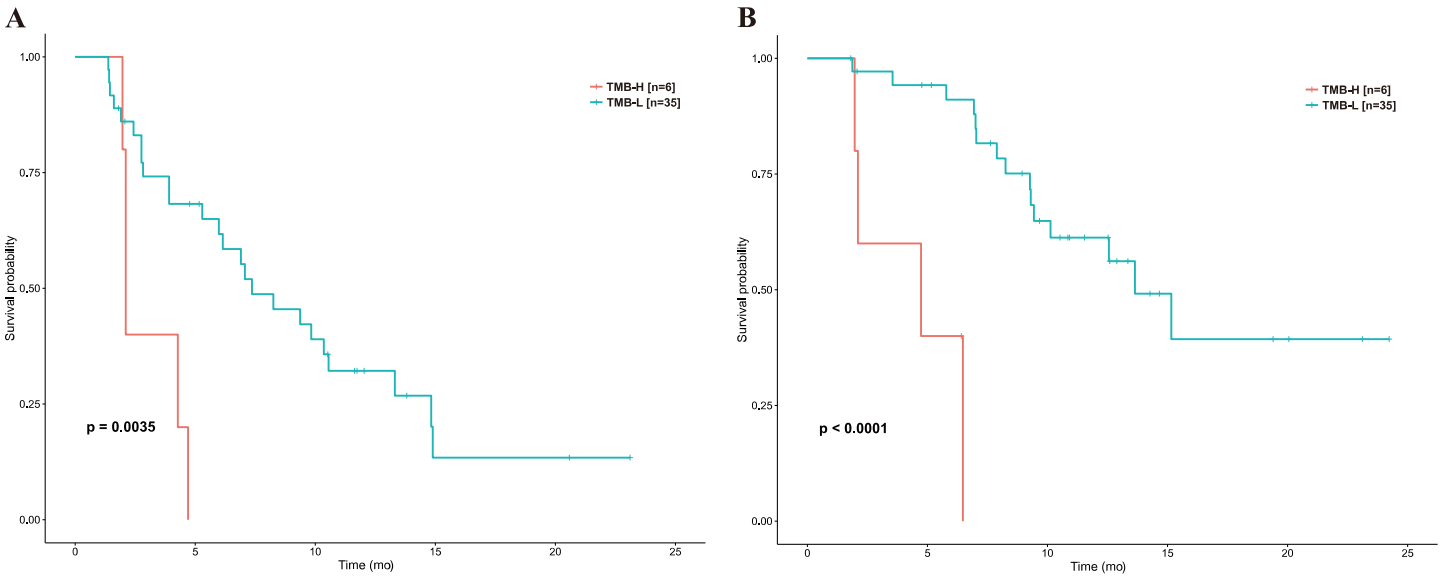

Figure 14. The Kaplan-Meier plot for low and high TMB thresholds.

(A) The right plot shows the PFS of the TMB groups. (B) The left plot shows the OS of the TMB groups. The red line indicates the TMB-H group, and the blue line indicates the TMB-L group. TMB-L; low tumor mutation burden, TMB-H; high tumor mutation burden, PFS; progression free survival, and OS; overall survival.

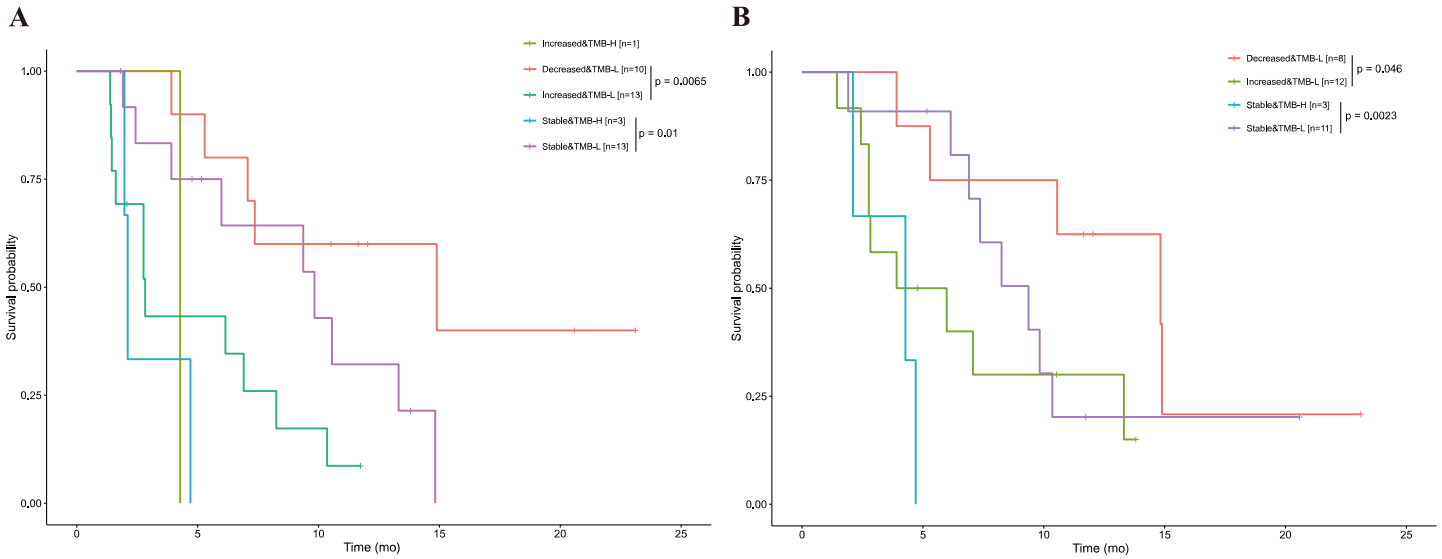

Figure 15. The Kaplan-Meier plot for a combined threshold.

The TMB-L and TMB-H groups were distinguished by a specific threshold. (A) The right plot shows the PFS of the TMB groups. (B) The left plot shows the OS of the TMB groups. The red line indicates the TMB-H group, and the blue line indicates the TMB-L group. TMB-L; low tumor mutation burden, TMB-H; high tumor mutation burden, PFS; progression free survival, and OS; overall survival.

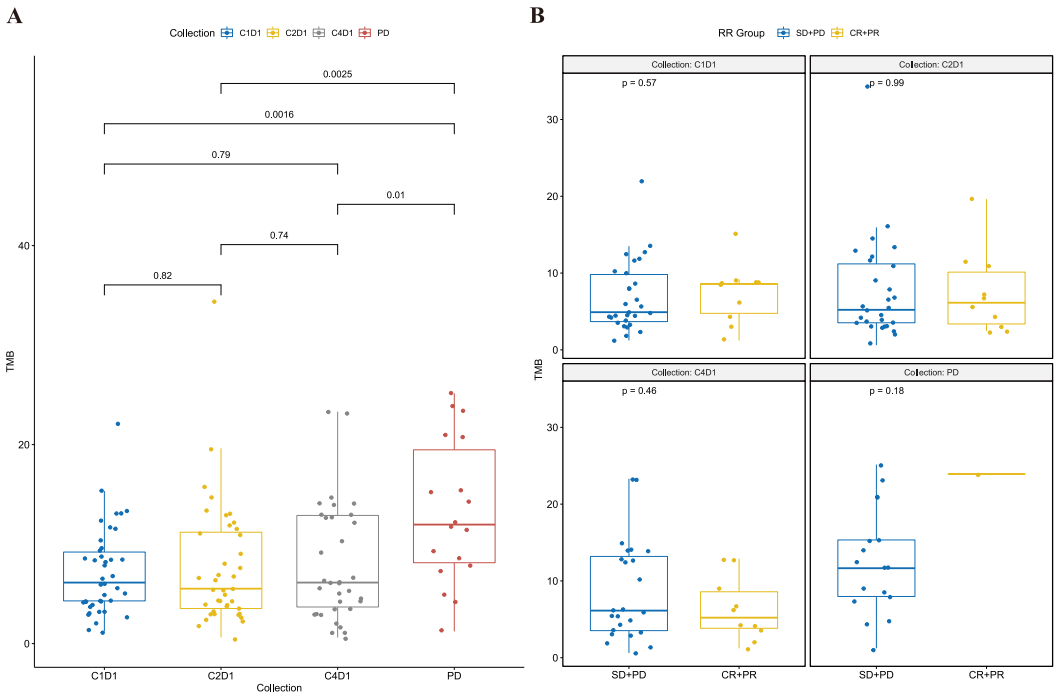

Figure 16. Comparison of the TMB level at each timepoint with clinical features.

The left box plot shows the comparison of the TMB level from each timepoint. (B) The right box plot indicates the comparison of the TMB levels by the response rate groups. C1D1; pre-1st chemotherapy, C2D1; pre-2nd chemotherapy, C4D1; pre-4th chemotherapy, PD; progression diseases, CR; complete response, PR; partial response, SD; stable disease

11. Comparison of the cfDNA amount at each timepoint with clinical features

We validated the potential use of cfDNA as a prognosis marker in BTC. When the cfDNA amount was compared at each timepoint, we observed an increased cfDNA quantity in progression disease. However, significant changes were not identified between timepoints except for the pre-4th chemotherapy versus progression disease (Figure 17A). We also compared the cfDNA level between response rate groups (CR+PR and SD+PD). An increased amount of cfDNA in progression disease was observed, but no significant differences were confirmed (Figure 17B). Also, there was no significant difference in the cfDNA amount between the TMB-H and TMB-L groups (Figure 17C).

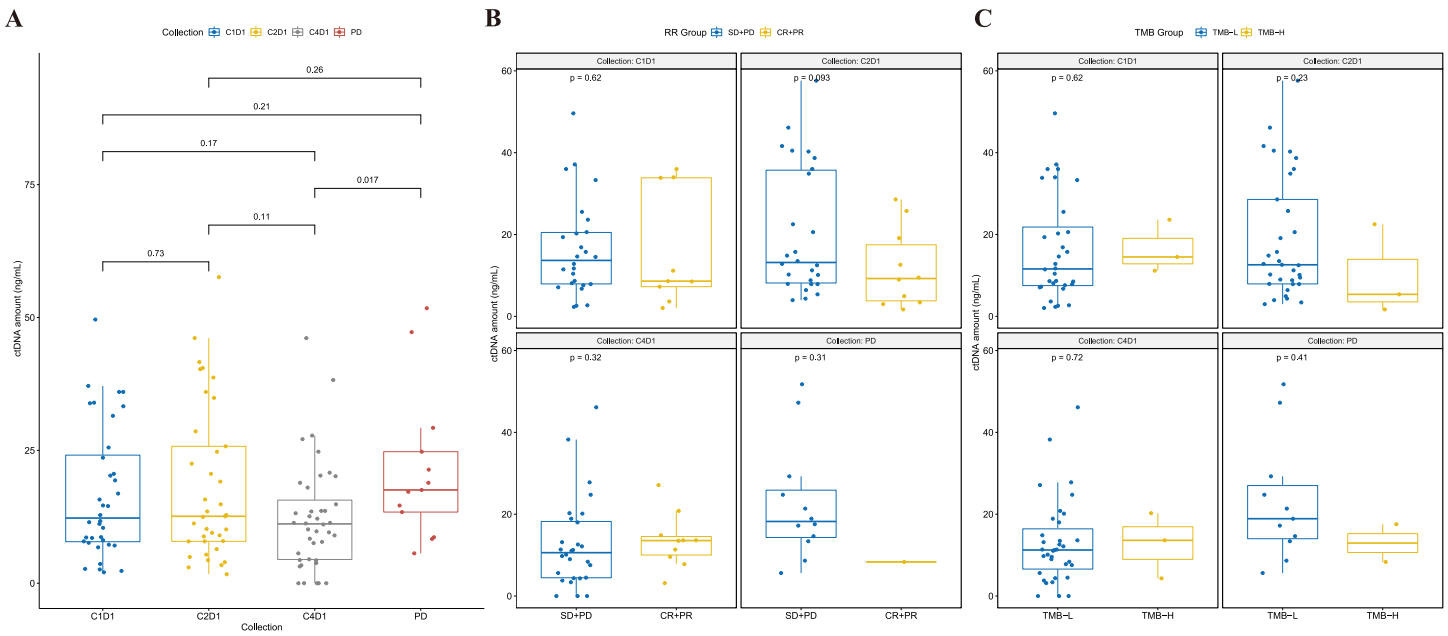

Figure 17. Comparison of the cfDNA amount at each timepoint with clinical features.

(A) The left box plot shows a comparison of the cfDNA amount from each timepoint. (B) The middle box plot indicates a comparison of the cfDNA amount by the response rate groups. (C) The right box plot shows a comparison of the cfDNA amount by the TMB group. C1D1; pre-1st chemotherapy, C2D1; pre-2nd chemotherapy, C4D1; pre-4th chemotherapy, PD; progression diseases, CR; complete response, PR; partial response, SD; stable disease.

IV. DISCUSSION

We compared our data and high frequency genes of BTC from the cBioPortal data. In the cBioPortal, *TP53* (27.6 %), *ARID1A* (17.6 %), *IDH1* (13.9 %), *BAP1* (12.9 %), *KRAS* (10.4 %), *MUC16* (12.1 %), *PBRM1* (9.5 %), *SMAD4* (8.4 %), and *ATM* (6.0 %) mutations were highly frequent. We recognized that the above genes were contained in our mutational profiles. Specially, *TP53* and AT-Rich Interactive Domain (*ARID*) genes highly corresponded between our data and the cBioPortal data. It was assumed that shared gene mutations may be the potential driver genes in BTC. Detected genes including *TP53* and *ARID* family genes were categorized into several key cancer pathways. The terms 'Epigenetic regulation,' 'TP53 signaling,' 'RAS/RAF/ERK pathway,' 'PI3K/AKT/mTOR pathway,' 'DNA damage,' 'Angiogenesis,' and 'DNA repair' were highly ranked. The high frequency of epigenetic regulation genes, including *ARID2*, *ARID1A*, *ARID1B*, *IDH1*, *KMT2A*, *PBRM1*, *BAP1*, and *TET1*, implied the importance of epigenetic alteration in BTC. DNA modification, RNA modification, miRNA biogenesis, chromatin remodeling, and histone acetylation, phosphorylation, ubiquitination, and methylation are known as genomic alterations of epigenetic regulators in BTC[76]. Among them, DNA methylation is a well-established mechanism of epigenetic regulation. In cancer, promoter regions of tumor suppressor genes are silenced through DNA methylation. Silencing of tumor suppressor genes induced impaired pathway functions, such as the DNA damage response, cell cycle, DNA repair, and cell death[77]. The SWI/SNF complex, which controls the chromatin remodeling process, contains several proteins encoded by *ARID1A*, *ARID1B*, *BAP1*, and *PBRM1*[78-80]. These genes frequently occur in BTC patients, and the loss of SWI/SNF member expression contributes to BTC obtaining an invasive phenotype in the late event of carcinogenesis[76].

BTC is comprised of three main types based on anatomical location: GBC, IHCCA, and EHCCA, which share different genetic backgrounds. Nakamura *et al*. reported the BTC mutational profiling of a large cohort (n = 260) with whole exome sequencing[80]. According to the literature, *FGFR2* mutations have been reported in IHCCA patients. In our cohort, we observed five patients with *FGFR2* mutations. Among these five

patients, one GBC patient (1/13 cases), one EHCCA patient (1/4 cases), and three IHCCA patients (3/11 cases) were distributed. In addition, *EGFR* family genes were frequently observed in GBC cases. Our cohort contained nine patients with *EGFR* family gene mutations, and four GBC patients (4/13 cases), one EHCCA patient (1/4 cases), and four IHCCA patients (4/23 cases). The four GBC patients had 73 % *EGFR* family gene mutations. The *KRAS* mutation was found more frequently in IHCCA and EHCCA than in GBC. Seven patients with *KRAS* mutations were observed in our cohort: one GBC patient (1/13 cases), two EHCCA patients (2/4 cases), and four IHCCA patients (4/23 cases). The *TP53* mutation was most frequently observed in our cohort. Interestingly, 77 % GBC patients (10/13 cases) had *TP53* mutations while 48 % IHCCA and EHCCA patients (13/27 cases) with *TP53* mutations were observed. Additionally, mutated *ARID1A* has been frequently observed in IHCCA. Six patients who had *ARID1A* mutations were found in our results. Among these patients, one GBC patient (1/13 cases) and five IHCCA patients (5/23 cases) were observed. However, the distribution of the *ARID2* mutation showed opposite results. Five GBC patients (5/13 cases) and four IHCCA patients (4/27 cases) had *ARID2* mutations. Also, the *MYC* and *MDM2* amplifications were frequently observed in IHCCA. Only one GBC patient (1/13 cases) and one EHCCA patient (1/27 cases) had the *MYC* amplification, while one IHCCA patient with the *MDM2* mutation was identified. All genomic spectra of the cancer subtypes were correlated with the literature except for the *MYC* amplification case.

The protein tyrosine phosphatases (PTPs) are involved in IL-6/STAT3 signaling[81]. PTPs have been implicated in tumorigenesis and progrssion[82]. PTPs comprised various enzymes encoded by 107 genes. Six gene mutations, *PTPRF*, *PTPRG*, *PTPRT*, *PTPN3*, *PTPN13*, and *PTPN14*, are the most commonly seen in human cancer. Among them, *PTPRT* was highly mutated in lung and gastric cancers[83] the *PTPRT* mutation altered the function which directly dephosphorylated STAT3 Y705 in colorectal cancer (CRC) cell lines treated with IL-6[84]. The PTPRT protein mainly consisted of meprin and the A-5 protein, as well as the receptor protein-tyrosine phosphatase mu (MAM) signature, fibronectin type III repeat (FN3) signature, immunoglobulin-like (Ig) signature, and protein tyrosine phosphatases (PTPc) signature. The MAM, Ig, and first two FN3

domains are required for efficient cell-cell adhesion[85-88]. Mutations in the PTPc domains reduced the phosphatase activity of *PTPRT*[83], which was related with tumorigenesis. This evidence supports the idea that the *PTPRT* mutation serves cancer progression and metastasis. As shown in Figure 5, the *PTPRT* mutation was significantly increased in the progression disease timepoint as compared with other timepoints. Mutations of *PTPRT* (S696Y, V750M, and R862Q) occurred in pre-1st chemotherapy and *PTPRT* (E181K, E468K, D595N, P1079T, A1096G, and R1188C) mutations were newly acquired in progression disease. In head and neck cancer (HNSCC), *PTPRT* mutations have been reported in 10 of 22 HNSCC patients[89]. In the study, the *PTPRT* mutation on the MAM and FN3 domains exactly matched that in our study (E181K and E468K). Also, the *PTPRT* mutations reported on the PTPc domains were located near mutations seen in our study (P1075L–P1079T and I1097V–A1096G). Specifically, we assumed that *PTPRT* (E181K) on the MAM domain, *PTPRT* (E489K) on the FN3 domain, and *PTPRT* (P1079T, A1096G, and R1188C) on the PTPc domains have a potential relationship with cancer progression. Hypermethylation of the *PTPRT* promoter region affected carcinogenesis in sporadic colorectal cancer[90]. Among 95 control samples, no methylated samples were observed. However, 108 of 131 cancer samples showed a hypermethylated status. *PTPRT* has been studied in other cancer types, such as HNCCS and CRC. However, BTC studies associated with the *PTPRT* mutation are very rare. We found two recently published BTC studies. Chung T *et al*. reported that IHCCA with ductal plate malformation (n = 5) has the *FGFR2* and *PTPRT* mutations as the most frequent variants[91]. Xue R *et al*. suggested that the WGS data of 74 tumors (combined hepatocellular and intrahepatic cholangiocarcinoma) showed that 80 % of tumor single cells have *PTPRT* mutations[92].

GemCis as a first-line regimen is currently a standard treatment for patients with unresectable BTC. We thought that the persistence pattern of PDR genes in patients under chemotherapy affected their prognosis. Klco JM *et al*. reported that persistent gene mutations associated with acute myeloid leukemia (AML) in patients with AML after chemotherapy is critical upon prognosis evaluation[93]. They observed that patients with a clearance pattern had no mutations (cut off was VAF < 2.5 %) while patients

with a persistence pattern had at least one mutation (VAF ≥ 2.5 %). Patients with a clearance pattern showed significantly higher median PFS than the persistence pattern group (17.9 mo versus 6.0 mo, $p < 0.001$). However, utilization of this approach was not common; we could not find solid cancer studies that used the strategy. We assumed that tumor samples were easily collected from patients with blood cancers, such as AML. However, in the case of a solid tumor, repeated collection of tumor samples from patients under chemotherapy was difficult. The approach using cfDNA in solid cancer may have potential risk stratification for the patient although many future studies are needed.

Cisplatin cross-links double-stranded DNA. The adducts induce inhibition of DNA replication and transcription and lead to cell cycle arrest and the DNA damage response[94]. In cancer cells, continuous treatment with cisplatin induced anti-apoptosis via various signaling networks, such as TP53, MAPK, FAS, PI3K, NF-kB, and the STAT3 pathway[95]. In our results, we detected several genes of PDR (*TP53*, *ATM*, *CDKN1A*, *CDKN2A*, *ERCC1*, *PIK3CA*, *PIK3CB*, *PIK3CD*, *PIK3R1*, *BCL2L1*, *BRCA1*, *ERBB2*, *MAPK1*, *MAPK3*, *MSH6*, *BIRC3*, and *CAP8*). The inactivated form of *TP53* has been reported in many cancer patients and is associated with resistance to drugs, including cisplatin, temozolomide, doxorubicin, gemcitabine, tamoxifen, and cetuximab[96]. Mutated *TP53* inhibits the cell cycle and apoptosis, which involves the *CDKN* family genes and the *ATM* gene[97]. *ERCC1* is a critical gene in the nucleotide excision repair (NER) process[98]. Genes encoding PI3K also participate heavily in the cell cycle, quiescence, and proliferation. An abnormally activated PI3K pathway induces chemoresistance and metastasis, and it inhibits BCL2 family protein-induced apoptosis[99]. *BRCA1* contributes genomic stability through DNA repair, cell cycle, ubiquitination cycle, chromatin structure regulation, and transcription regulation. In particular, *BRCA1* participates in homologous recombination (HR). Chemosensitivity has been reported in cancer patients with mutated *BRCA1* when they are treated with drugs at the initial stage, but gene functions restored via secondary *BRCA* mutations and complex interactions with other DNA repair genes induce PDR[100]. *ERBB2* is one of the *EGFR* family members and it contributes to PDR through PI3K and the

RAS/MAPK pathway. *ERBB* dependent PI3K and RAS/MAPK pathways enhanced PDR by apoptosis inhibition that was induced via the phosphorylated BAD protein[101]. *MSH6* encoded one of the mismatch repair (MMR) proteins. A mutated MMR protein could not recognize DNA damage by cisplatin, which induced PDR. Also, the *BIRC3* gene was involved in the NF-kB pathway and this anti-apoptotic gene along with *BCL2*, *BCL2L2*, and *MCL1* promoted cisplatin resistance[102]. According to a functional study, *CASP8* along with *CASP3* and *CASP6* participated in cisplatin-specific apoptosis signaling. *CASP8* is a key molecule regulated by *CASP3* and *CASP6* at the initial cascade step[103].

As mentioned above, PDR genes are associated with DNA repair, cell cycle, and apoptosis through the PI3K, ERBB, and STAT3 pathways. These pathways are known potential targets for BTC patients.

The PI3K pathway was activated by EGFR, ERBB2, MET, VEGFR, and FGFR2 fusion. Overexpression of PI3K promoted activation of STAT3[104]. Also, inhibition of STAT3 through PI3K suppression increased autophagy activation, which decreased cisplatin resistance, tumor growth, and metastasis. Normal TP53 introduction inhibited expression of STAT3 and promoted cisplatin chemosensitivity[105]. The *PTPRT* that we proposed as a potential marker has a function for STAT3 regulation.

We suggested that patients in the non-persistent PDR group showed a reduced frequency of 'TP53 signaling' when compared between the pre-1st chemotherapy and other chemotherapy cycle (C2D1 and C4D1) timepoints, although there was no significance. Only one patient with mutated PI3K-associated genes was observed, and there were no patients with mutated STAT3-associated genes under chemotherapy. We assumed that the PI3K and STAT3 pathways may affect chemoresistance and cancer progression in BTC. Therefore, prognosis comparison was conducted between patient groups associated with the PI3K and STAT3 pathways. As shown in Figure 12, we identified two pathways that affected the prognosis of BTC patients. However, this result is one of little clues. To prove this assumption, more scientific evidence and further research are needed.

MSI has been considered as one of the useful biomarkers for immune checkpoint blockade therapy (ICB)[70]. BTC patients treated with Pembrolizumab, a U.S. FDA

approved MSI-high/mismatch repair-deficient solid cancer drug, showed a high response rate (CR 9 % and PR 32 % of a total 40.9 %) and overall survival (median OS 24.3 mo)[106]. However, in our results, we could not find any MIS-H patients. Studies reported a low frequency of MSI-H patients with BTC, and the frequency range was from 0 to 18.2 %[107-113]. Most studies suggested that there is under a 10 % frequency of BTC patients with the MSI-high status. Thus, MSI-H tumors are usually very rare in BTC.

The cfDNA amount has been considered as a prognosis marker. However, in our results, the cfDNA amount was not correlated with any clinical features. Although the cfDNA amount was increased in progression disease, significant changes were not observed according to response rate and TMB level. In lung cancer, the median cfDNA concentration was compared with the response rate groups and the study reported that the cfDNA concentration with chemotherapy response was not associated[49]. In fact, the cfDNA concentration was influenced by various biases, such as age, sample type, plasma separation method, and extraction kit[114]. In particular, chemotherapy-induced lysis of normal cells contributed to the cfDNA concentration. This is one of the main reasons why the total cfDNA concentration was not correlated with the response rate of chemotherapy[49].

The TMB level has been widely studied in cancer therapy. Although the threshold of TMB was not clearly established, cancer studies suggested > 10 TMB or a median TMB value as a threshold[115-117]. However, certain cancers have a very high or low level of average TMB, therefore, this threshold cannot be applied in all cases. We introduced a modified threshold by Fernandez EM *et al*.,[75] which showed that the PFS and OS rates were significantly different between the TMB-H and TMB-L groups. A high TMB level means more neoantigens, which were recognized by T-cell receptors, were present than in low TMB patients. It also indicated that TMB-H patients have more clinical benefits from the drug response. However, our opposing result showed a prolonged survival rate of the TMB-L group. According to the 2021 European Society for Medical Oncology (ESOM), among BTC patients, TMB-H patients receiving ICB treatment showed a lower survival rate than TMB-L patients with ICB treatment because CD8 T-cell infiltration is not positively correlated with neoantigens in BTC[116].

The TMB of cancer, which was negatively correlated with CD8 T-cell infiltration like BTC, showed the opposite clinical benefit trend for the anti-tumor drug. In a study of 20 primary solid cancer types from The Cancer Genome Atlas (TCGA) with 6,305 patients, BTC, adrenocortical carcinoma, colon adenocarcinoma, esophageal carcinoma, renal clear cell carcinoma, hepatocellular carcinoma, mesothelioma, and pancreatic adenocarcinoma showed better prognosis when these cancer patients had a high TMB status. On the other hand, high TMB predicted a prolonged prognosis of bladder urothelial carcinoma, renal papillary cell carcinoma, stomach adenocarcinoma, endocervical adenocarcinoma, ovarian serous cystadenocarcinoma, and uterine corpus endometrial carcinoma[118].

To our knowledge, Jiang T *et al*. first reported the dTMB threshold in 2022[119]. In the study, the authors showed that dTMB was a valuable prognostic biomarker for patients with lung cancer under camrelizumab plus chemotherapy. Also, they suggested that the combination of different TMB cutoffs was highly correlated with patient prognosis. We first suggested dTMB for patients with BTC. Among three thresholds for dTMB (Figure 13), 20 % increased dTMB / 30 % decreased dTMB was the most significant threshold at C1D1–C2D1 and C1D1–C4D1 (Figure 13C and D). The cutoff is correlated with the Response Evaluation Criteria in Solid Tumours (RECIST) 1.1 guideline[62]. In the guideline, definitions of partial response and progressive disease are “At least a 30 % decrease in the sum of diameters of target lesions, taking as reference the baseline sum diameters” and “At least a 20 % increase in the sum of diameters of target lesions, taking as reference the smallest sum on study”. This evidence supported that the threshold is clinically and statistically reasonable. Prognosis prediction using a combination of the two mentioned thresholds showed improved performance; these thresholds complemented each other. We showed statistically significant results using dTMB and a combination of thresholds; however, these approaches are not common. Accumulation of the scientific evidence about dTMB is highly necessary, and through this, more clinical and statistical thresholds should be suggested.

FGFR2 fusions with a prevalence of 10–15 % in BTC have been reported[120]. Pemigatinib is an inhibitor for *FGFR2* fusion rearrangement and is a target therapy,

which was approved by the U.S. FDA in BTC patients[25, 121]. During diagnosis, selection of patients harboring a *FGFR2* fusion is important for appropriate treatment. The *FGFR2* fusion has many potential partner genes (at least 150 in BTC). Because of the large number of partner genes, the traditional RT-PCR method is not practicable[121]. Consequently, the best option is RNA-seq. Although cfDNA NGS is another feasibly complementary technique, it has limitations on the detection of the *FGFR2* fusion. Goyal L *et al*. reported a study on *FGFR2* fusion in BTC using cfDNA NGS[122]. Among 84 participants in the NCT02160041 (BGJ398) clinical trial, three patients with advanced *FGFR2* fusion-positive BTC were analyzed with the Guardant 360 assay for cfDNA. Each patient harbored *FGFR2-ZMYM4*, *FGFR2-OPTN*, and *FGFR2-BICC1* fusions in tissue NGS. Only the patient with a *FGFR2-BICC1* fusion was *FGFR2* fusion-positive in cfDNA NGS. Berchuck JE *et al*. reported cfDNA landscape alterations in 1,671 patients with BTC using the Guardant 360 cfDNA NGS assay[123]. In the study, the authors showed that significantly different detection rates of *FGFR2* fusion between cfDNA and tissue samples (1.4 % and 4.3 %; p = 0.0018) were observed. Only 18 % of patients (12/67) with *FGFR2* fusion detected in tissue NGS were identified in cfDNA samples. The authors mentioned that low ctDNA shedding could not explain the low detection rate of *FGFR2* fusion, and the *FGFR2* fusion partner gene was correlated with the detection rate. A total of 42 unique partner genes were identified in tissue samples, and the *BICC1* gene (28.4 %) was the most common partner of *FGFR2* fusion. Among the *FGFR2-BICC1* fusions detected in tissue samples, 58 % were confirmed in cfDNA samples. However, 2.1 % of non-*BICC1* fusions (1/48; *FGFR2-TACC2*) were observed in cfDNA. Also, the authors assessed the *FGFR2* fusion detection rate in 259 serial cfDNA samples (n = 35, *BICC1* = 6, non-*BICC1* = 29). Among six *FGFR2-BICC1* fusion-positive patients, the *FGFR2-BICC1* fusion was detected in all samples of the three patients. The *FGFR2-BICC1* fusions of three other patients were not detected in all samples or any following samples. The *FGFR2* fusions with non-*BICC1* partners were not detected in any serial cfDNA samples.

The results of our pilot experiment about *FGFR2* fusion detection in cfDNA NGS were correlated with the above research. Six unique *FGFR2* fusions were identified by

tissue NGS (partner genes; *TACC2*, *NOL4*, *MPP1*, *DUSP6*, *POC1B*, and *KIAA1217*) in six patients. All *FGFR2* fusions were non-*BICC1* partner mutations, and five unique *FGFR2* fusions were not detected in cfDNA NGS except for *FGFR2-TACC2*. The result correlated with the detection of non-*FGFR2-BICC1* fusion from the Berchuck JE *et al*. study. This evidence indicates that an integrated approach using tissue biopsy and liquid biopsy is important when researchers and clinicians determine an absence of *FGFR2* fusion in BTC patients.

V. CONCLUSION

The present study enrolled a large prospective BTC cohort and used a large pan-cancer gene panel. We suggested utilizing cfDNA NGS through liquid biopsy based on its high concordance with tissue NGS. We provided the key pathways and mutated genes from mutational profiling of unresectable BTC patients in multiple timepoints while under chemotherapy. Through our data, actionable candidates and molecular mechanisms of BTC were proposed. Estimation of TMB using cfDNA NGS showed high performance for prognosis prediction. Although we could not fully explain the molecular mechanism of BTC, our results provide molecular knowledge for BTC patients.

REFERENCES

1. Benavides M, Anton A, Gallego J, Gomez MA, Jimenez-Gordo A, La Casta A, *et al*. Biliary tract cancers: SEOM clinical guidelines. Clin Transl Oncol 2015;17(12):982-7.
2. Lazcano-Ponce EC, Miquel JF, Munoz N, Herrero R, Ferrecio C, Wistuba, II, *et al*. Epidemiology and molecular pathology of gallbladder cancer. CA Cancer J Clin 2001;51(6):349-64.
3. Wistuba, II and Gazdar AF. Gallbladder cancer: lessons from a rare tumour. Nat Rev Cancer 2004;4(9):695-706.
4. Personeni N, Lleo A, Pressiani T, Colapietro F, Openshaw MR, Stavraka C, *et al*. Biliary tract cancers: molecular heterogeneity and new treatment options. Cancers (Basel) 2020;12(11):3370.
5. Bertuccio P, Malvezzi M, Carioli G, Hashim D, Boffetta P, El-Serag HB, *et al*. Global trends in mortality from intrahepatic and extrahepatic cholangiocarcinoma. J Hepatol 2019;71(1):104-14.
6. Patel T. Increasing incidence and mortality of primary intrahepatic cholangiocarcinoma in the United States. Hepatol 2001;33(6):1353-7.
7. Sripa B, Kaewkes S, Sithithaworn P, Mairiang E, Laha T, Smout M, *et al*. Liver fluke induces cholangiocarcinoma. PLoS Med 2007;4(7):e201.
8. Lindner P, Rizell M, and Hafstrom L. The impact of changed strategies for patients with cholangiocarcinoma in this millenium. HPB Surg 2015;2015:736049.
9. Kamsa-Ard S, Luvira V, Suwanrungruang K, Kamsa-Ard S, Luvira V, Santong C, *et al*. Cholangiocarcinoma trends, incidence, and relative survival in Khon Kaen, Thailand From 1989 through 2013: A Population-Based Cancer Registry Study. J Epidemiol 2019;29(5):197-204.
10. Strijker M, Belkouz A, van der Geest LG, van Gulik TM, van Hooft JE, de Meijer VE, *et al*. Treatment and survival of resected and unresected distal cholangiocarcinoma: a nationwide study. Acta Oncol 2019;58(7):1048-55.
11. Alabraba E, Joshi H, Bird N, Griffin R, Sturgess R, Stern N, *et al*. Increased multimodality treatment options has improved survival for hepatocellular carcinoma but poor survival for biliary tract cancers remains unchanged. Eur J Surg Oncol 2019;45(9):1660-7.
12. Groot Koerkamp B, Wiggers JK, Allen PJ, Besselink MG, Blumgart LH, Busch OR, *et al*. Recurrence rate and pattern of perihilar cholangiocarcinoma after curative intent resection. J Am Coll Surg 2015;221(6):1041-9.
13. Komaya K, Ebata T, Yokoyama Y, Igami T, Sugawara G, Mizuno T, *et al*. Recurrence after curative-intent resection of perihilar cholangiocarcinoma: analysis of a large cohort with a close postoperative follow-up approach. Surgery 2018;163(4):732-8.
14. Cambridge WA, Fairfield C, Powell JJ, Harrison EM, Soreide K, Wigmore SJ, *et al*. Meta-analysis and meta-regression of survival after liver transplantation for unresectable perihilar cholangiocarcinoma. Ann Surg 2021;273(2):240-50.
15. Spolverato G, Kim Y, Alexandrescu S, Marques HP, Lamelas J, Aldrighetti L, *et al*. Management and outcomes of patients with recurrent intrahepatic cholangiocarcinoma following previous curative-intent surgical resection. Ann Surg Oncol 2016;23(1):235-43.
16. Oh JK and Weiderpass E. Infection and cancer: global distribution and burden of diseases. Ann Glob Health 2014;80(5):384-92.
17. Sripa B, Tangkawattana S, and Brindley PJ. Update on pathogenesis of opisthorchiasis and cholangiocarcinoma. Adv Parasitol 2018;102:97-113.

18. Rizvi S, Khan SA, Hallemeier CL, Kelley RK, and Gores GJ. Cholangiocarcinoma - evolving concepts and therapeutic strategies. Nat Rev Clin Oncol 2018;15(2):95-111.
19. Khan SA, Tavolari S, and Brandi G. Cholangiocarcinoma: epidemiology and risk factors. Liver Int 2019;39 Suppl 1:19-31.
20. Schmidt MA, Marcano-Bonilla L, and Roberts LR. Gallbladder cancer: epidemiology and genetic risk associations. Chin Clin Oncol 2019;8(4):31.
21. Banales JM, Marin JJG, Lamarca A, Rodrigues PM, Khan SA, Roberts LR, *et al*. Cholangiocarcinoma 2020: the next horizon in mechanisms and management. Nat Rev Gastroenterol Hepatol 2020;17(9):557-88.
22. Wang H, Sun P, and Baria K. The world-wide incidence of biliary tract cancer (BTC). JCO 2020;38(4_suppl):585.
23. Modolell I, Guarner L, and Malagelada JR. Vagaries of clinical presentation of pancreatic and biliary tract cancer. Ann Oncol 1999;10 Suppl 4:82-4.
24. Valle J, Wasan H, Palmer DH, Cunningham D, Anthoney A, Maraveyas A, *et al*. Cisplatin plus gemcitabine versus gemcitabine for biliary tract cancer. N Engl J Med 2010;362(14):1273-81.
25. Abou-Alfa GK, Sahai V, Hollebecque A, Vaccaro G, Melisi D, Al-Rajabi R, *et al*. Pemigatinib for previously treated, locally advanced or metastatic cholangiocarcinoma: a multicentre, open-label, phase 2 study. Lancet Oncol 2020;21(5):671-84.
26. Goyal L, Meric-Bernstam F, Hollebecque A, Valle JW, Morizane C, Karasic TB, *et al*. FOENIX-CCA2: a phase II, open-label, multicenter study of futibatinib in patients (pts) with intrahepatic cholangiocarcinoma (iCCA) harboring FGFR2 gene fusions or other rearrangements. JCO 2020;38(15_suppl):108.
27. Makawita S, G KA-A, Roychowdhury S, Sadeghi S, Borbath I, Goyal L, *et al*. Infigratinib in patients with advanced cholangiocarcinoma with FGFR2 gene fusions/translocations: the PROOF 301 trial. Future Oncol 2020;16(30):2375-84.
28. Javle MM, Roychowdhury S, Kelley RK, Sadeghi S, Macarulla T, Waldschmidt DT, *et al*. Final results from a phase II study of infigratinib (BGJ398), an FGFR-selective tyrosine kinase inhibitor, in patients with previously treated advanced cholangiocarcinoma harboring an FGFR2 gene fusion or rearrangement. JCO 2021;39(3_suppl):265.
29. Abou-Alfa GK, Macarulla T, Javle MM, Kelley RK, Lubner SJ, Adeva J, *et al*. Ivosidenib in IDH1-mutant, chemotherapy-refractory cholangiocarcinoma (ClarIDHy): a multicentre, randomised, double-blind, placebo-controlled, phase 3 study. Lancet Oncol 2020;21(6):796-807.
30. Gomez-Roca C, Yanez E, Im S-A, Alvarez EC, Senellart H, Doherty M, *et al*. LEAP-005: a phase II multicohort study of lenvatinib plus pembrolizumab in patients with previously treated selected solid tumors—results from the colorectal cancer cohort. JCO 2021;39(3_suppl):94.
31. Khan SA, Thomas HC, Davidson BR, and Taylor-Robinson SD. Cholangiocarcinoma. Lancet 2005;366(9493):1303-14.
32. Patel AH, Harnois DM, Klee GG, LaRusso NF, and Gores GJ. The utility of CA 19-9 in the diagnoses of cholangiocarcinoma in patients without primary sclerosing cholangitis. Am J Gastroenterol 2000;95(1):204-7.
33. Hultcrantz R, Olsson R, Danielsson A, Jarnerot G, Loof L, Ryden BO, *et al*. A 3-year prospective study on serum tumor markers used for detecting cholangiocarcinoma in patients with primary sclerosing cholangitis. J Hepatol 1999;30(4):669-73.
34. Abbas G and Lindor KD. Cholangiocarcinoma in primary sclerosing cholangitis. J

Gastrointest Cancer 2009;40(1-2):19-25.
35. Park MS, Kim TK, Kim KW, Park SW, Lee JK, Kim JS, *et al*. Differentiation of extrahepatic bile duct cholangiocarcinoma from benign stricture: findings at MRCP versus ERCP. Radiology 2004;233(1):234-40.
36. Banales JM, Cardinale V, Carpino G, Marzioni M, Andersen JB, Invernizzi P, *et al*. Expert consensus document: cholangiocarcinoma: current knowledge and future perspectives consensus statement from the European Network for the Study of Cholangiocarcinoma (ENS-CCA). Nat Rev Gastroenterol Hepatol 2016;13(5):261-80.
37. Schwarzenbach H, Hoon DS, and Pantel K. Cell-free nucleic acids as biomarkers in cancer patients. Nat Rev Cancer 2011;11(6):426-37.
38. Celec P, Vlkova B, Laukova L, Babickova J, and Boor P. Cell-free DNA: the role in pathophysiology and as a biomarker in kidney diseases. Expert Rev Mol Med 2018;20:e1.
39. Thierry AR, Mouliere F, Gongora C, Ollier J, Robert B, Ychou M, *et al*. Origin and quantification of circulating DNA in mice with human colorectal cancer xenografts. Nucleic Acids Res 2010;38(18):6159-75.
40. Garcia Moreira V, de la Cera Martinez T, Gago Gonzalez E, Prieto Garcia B, and Alvarez Menendez FV. Increase in and clearance of cell-free plasma DNA in hemodialysis quantified by real-time PCR. Clin Chem Lab Med 2006;44(12):1410-5.
41. Gauthier VJ, Tyler LN, and Mannik M. Blood clearance kinetics and liver uptake of mononucleosomes in mice. J Immunol 1996;156(3):1151-6.
42. Yan YY, Guo QR, Wang FH, Adhikari R, Zhu ZY, Zhang HY, *et al*. Cell-free DNA: hope and potential application in cancer. Front Cell Dev Biol 2021;9:639233.
43. Alcaide M, Cheung M, Hillman J, Rassekh SR, Deyell RJ, Batist G, *et al*. Evaluating the quantity, quality and size distribution of cell-free DNA by multiplex droplet digital PCR. Sci Rep 2020;10(1):12564.
44. Kustanovich A, Schwartz R, Peretz T, and Grinshpun A. Life and death of circulating cell-free DNA. Cancer Biol Ther 2019;20(8):1057-67.
45. Aucamp J, Bronkhorst AJ, Badenhorst CPS, and Pretorius PJ. The diverse origins of circulating cell-free DNA in the human body: a critical re-evaluation of the literature. Biol Rev Camb Philos Soc 2018;93(3):1649-83.
46. Ungerer V, Bronkhorst AJ, Van den Ackerveken P, Herzog M, and Holdenrieder S. Serial profiling of cell-free DNA and nucleosome histone modifications in cell cultures. Sci Rep 2021;11(1):9460.
47. Eskandari M, Manoochehrabadi S, Pashaiefar H, Zaimy MA, and Ahmadvand M. Clinical significance of cell-free DNA as a prognostic biomarker in patients with diffuse large B-cell lymphoma. Blood Res 2019;54(2):114-9.
48. Kamat AA, Baldwin M, Urbauer D, Dang D, Han LY, Godwin A, *et al*. Plasma cell-free DNA in ovarian cancer: an independent prognostic biomarker. Cancer 2010;116(8):1918-25.
49. Tissot C, Toffart AC, Villar S, Souquet PJ, Merle P, Moro-Sibilot D, *et al*. Circulating free DNA concentration is an independent prognostic biomarker in lung cancer. Eur Respir J 2015;46(6):1773-80.
50. Cheng J, Holland-Letz T, Wallwiener M, Surowy H, Cuk K, Schott S, *et al*. Circulating free DNA integrity and concentration as independent prognostic markers in metastatic breast cancer. Breast Cancer Res Treat 2018;169(1):69-82.
51. Chan KC, Lai PB, Mok TS, Chan HL, Ding C, Yeung SW, *et al*. Quantitative analysis of circulating methylated DNA as a biomarker for hepatocellular carcinoma. Clin Chem

2008;54(9):1528-36.
52. Hendriks RJ, Dijkstra S, Smit FP, Vandersmissen J, Van de Voorde H, Mulders PFA, *et al*. Epigenetic markers in circulating cell-free DNA as prognostic markers for survival of castration-resistant prostate cancer patients. Prostate 2018;78(5):336-42.
53. Tham C, Chew M, Soong R, Lim J, Ang M, Tang C, *et al*. Postoperative serum methylation levels of TAC1 and SEPT9 are independent predictors of recurrence and survival of patients with colorectal cancer. Cancer 2014;120(20):3131-41.
54. Philipp AB, Stieber P, Nagel D, Neumann J, Spelsberg F, Jung A, *et al*. Prognostic role of methylated free circulating DNA in colorectal cancer. Int J Cancer 2012;131(10):2308-19.
55. Wallner M, Herbst A, Behrens A, Crispin A, Stieber P, Goke B, *et al*. Methylation of serum DNA is an independent prognostic marker in colorectal cancer. Clin Cancer Res 2006;12(24):7347-52.
56. Hussein NA, Mohamed SN, and Ahmed MA. Plasma ALU-247, ALU-115, and cfDNA integrity as diagnostic and prognostic biomarkers for breast cancer. Appl Biochem Biotechnol 2019;187(3):1028-45.
57. Panagopoulou M, Karaglani M, Balgkouranidou I, Biziota E, Koukaki T, Karamitrousis E, *et al*. Circulating cell-free DNA in breast cancer: size profiling, levels, and methylation patterns lead to prognostic and predictive classifiers. Oncogene 2019;38(18):3387-401.
58. Zill OA, Greene C, Sebisanovic D, Siew LM, Leng J, Vu M, *et al*. Cell-free DNA next-generation sequencing in pancreatobiliary carcinomas. Cancer Discov 2015;5(10):1040-8.
59. Rothwell DG, Ayub M, Cook N, Thistlethwaite F, Carter L, Dean E, *et al*. Utility of ctDNA to support patient selection for early phase clinical trials: the TARGET study. Nat Med 2019;25(5):738-43.
60. Ettrich TJ, Schwerdel D, Dolnik A, Beuter F, Blatte TJ, Schmidt SA, *et al*. Genotyping of circulating tumor DNA in cholangiocarcinoma reveals diagnostic and prognostic information. Sci Rep 2019;9(1):13261.
61. Okamura R, Kurzrock R, Mallory RJ, Fanta PT, Burgoyne AM, Clary BM, *et al*. Comprehensive genomic landscape and precision therapeutic approach in biliary tract cancers. Int J Cancer 2021;148(3):702-12.
62. Eisenhauer EA, Therasse P, Bogaerts J, Schwartz LH, Sargent D, Ford R, *et al*. New response evaluation criteria in solid tumours: revised RECIST guideline (version 1.1). Eur J Cancer 2009;45(2):228-47.
63. Alborelli I, Bratic Hench I, Chijioke O, Prince SS, Bubendorf L, Leuenberger LP, *et al*. Robust assessment of tumor mutational burden in cytological specimens from lung cancer patients. Lung Cancer 2020;149:84-9.
64. Allgauer M, Budczies J, Christopoulos P, Endris V, Lier A, Rempel E, *et al*. Implementing tumor mutational burden (TMB) analysis in routine diagnostics-a primer for molecular pathologists and clinicians. Transl Lung Cancer Res 2018;7(6):703-15.
65. Lee KS, Seo J, Lee C-K, Shin S, Choi Z, Min S, *et al*. Analytical and clinical validation of cell-free circulating tumor DNA Assay for the estimation of tumor mutational burden. Clin Chem 2022;68(12):1519-28.
66. Li H. Toward better understanding of artifacts in variant calling from high-coverage samples. Bioinformatics 2014;30(20):2843-51.
67. Li MM, Datto M, Duncavage EJ, Kulkarni S, Lindeman NI, Roy S, *et al*. Standards and guidelines for the interpretation and reporting of sequence variants in cancer: a joint consensus recommendation of the Association for Molecular Pathology, American Society of Clinical Oncology, and College of American Pathologists. J Mol Diagn 2017;19(1):4-

23.
68. Richards S, Aziz N, Bale S, Bick D, Das S, Gastier-Foster J, *et al*. Standards and guidelines for the interpretation of sequence variants: a joint consensus recommendation of the American College of Medical Genetics and Genomics and the Association for Molecular Pathology. Genet Med 2015;17(5):405-24.
69. Li K, Luo H, Huang L, Luo H, and Zhu X. Microsatellite instability: a review of what the oncologist should know. Cancer Cell Int 2020;20:16.
70. Rizzo A, Ricci AD, and Brandi G. PD-L1, TMB, MSI, and other predictors of response to immune checkpoint inhibitors in biliary tract cancer. Cancers (Basel) 2021;13(3).
71. Ciardiello D, Maiorano BA, Parente P, Rodriquenz MG, Latiano TP, Chiarazzo C, *et al*. Immunotherapy for biliary tract cancer in the era of precision medicine: current knowledge and future perspectives. Int J Mol Sci 2022;23(2).
72. Andre T, Shiu KK, Kim TW, Jensen BV, Jensen LH, Punt C, *et al*. Pembrolizumab in microsatellite-instability-high advanced colorectal cancer. N Engl J Med 2020;383(23):2207-18.
73. Lee M, Chun SM, Sung CO, Kim SY, Kim TW, Jang SJ, *et al*. Clinical utility of a fully automated microsatellite instability test with minimal hands-on time. J Pathol Transl Med 2019;53(6):386-92.
74. Zehir A, Benayed R, Shah RH, Syed A, Middha S, Kim HR, *et al*. Mutational landscape of metastatic cancer revealed from prospective clinical sequencing of 10,000 patients. Nat Med 2017;23(6):703-13.
75. Fernandez EM, Eng K, Beg S, Beltran H, Faltas BM, Mosquera JM, *et al*. Cancer-specific thresholds adjust for whole exome sequencing-based tumor mutational burden distribution. JCO Precis Oncol 2019;3:PO.18.00400.
76. O'Rourke CJ, Munoz-Garrido P, Aguayo EL, and Andersen JB. Epigenome dysregulation in cholangiocarcinoma. Biochimica et Biophysica Acta (BBA) - Molecular Basis of Disease 2018;1864(4, Part B):1423-34.
77. Esteller M, Corn PG, Baylin SB, and Herman JG. A gene hypermethylation profile of human cancer. Cancer Res 2001;61(8):3225-9.
78. Chan-On W, Nairismägi ML, Ong CK, Lim WK, Dima S, Pairojkul C, *et al*. Exome sequencing identifies distinct mutational patterns in liver fluke-related and non-infection-related bile duct cancers. Nat Genet 2013;45(12):1474-8.
79. Zou S, Li J, Zhou H, Frech C, Jiang X, Chu JS, *et al*. Mutational landscape of intrahepatic cholangiocarcinoma. Nat Commun 2014;5:5696.
80. Nakamura H, Arai Y, Totoki Y, Shirota T, Elzawahry A, Kato M, *et al*. Genomic spectra of biliary tract cancer. Nature Genetics 2015;47(9):1003-10.
81. Julien SG, Dube N, Hardy S, and Tremblay ML. Inside the human cancer tyrosine phosphatome. Nat Rev Cancer 2011;11(1):35-49.
82. Bessette DC, Qiu D, and Pallen CJ. PRL PTPs: mediators and markers of cancer progression. Cancer and Metastasis Reviews 2008;27(2):231-52.
83. Wang Z, Shen D, Parsons DW, Bardelli A, Sager J, Szabo S, *et al*. Mutational analysis of the tyrosine phosphatome in colorectal cancers. Science 2004;304(5674):1164-6.
84. Zhang X, Guo A, Yu J, Possemato A, Chen Y, Zheng W, *et al*. Identification of STAT3 as a substrate of receptor protein tyrosine phosphatase T. Proc Natl Acad Sci U S A 2007;104(10):4060-4.
85. Zondag GC, Koningstein GM, Jiang YP, Sap J, Moolenaar WH, and Gebbink MF. Homophilic interactions mediated by receptor tyrosine phosphatases mu and kappa. A

critical role for the novel extracellular MAM domain. J Biol Chem 1995;270(24):14247-50.

86. Cismasiu VB, Denes SA, Reiländer H, Michel H, and Szedlacsek SE. The MAM (meprin/A5-protein/PTPmu) domain is a homophilic binding site promoting the lateral dimerization of receptor-like protein-tyrosine phosphatase mu. J Biol Chem 2004;279(26):26922-31.
87. Aricescu AR, Hon WC, Siebold C, Lu W, van der Merwe PA, and Jones EY. Molecular analysis of receptor protein tyrosine phosphatase mu-mediated cell adhesion. Embo j 2006;25(4):701-12.
88. Aricescu AR, Siebold C, Choudhuri K, Chang VT, Lu W, Davis SJ, *et al*. Structure of a tyrosine phosphatase adhesive interaction reveals a spacer-clamp mechanism. Science 2007;317(5842):1217-20.
89. Lui VWY, Peyser ND, Ng PK-S, Hritz J, Zeng Y, Lu Y, *et al*. Frequent mutation of receptor protein tyrosine phosphatases provides a mechanism for STAT3 hyperactivation in head and neck cancer. Proc Natl Acad Sci USA 2014;111(3):1114-9.
90. Laczmanska I, Karpinski P, Bebenek M, Sedziak T, Ramsey D, Szmida E, *et al*. Protein tyrosine phosphatase receptor-like genes are frequently hypermethylated in sporadic colorectal cancer. J Hum Genet 2013;58(1):11-5.
91. Chung T, Rhee H, Shim HS, Yoo JE, Choi GH, Kim H, *et al*. Genetic, clinicopathological, and radiological features of intrahepatic cholangiocarcinoma with ductal plate malformation pattern. Gut Liver 2022;16(4):613-24.
92. Xue R, Chen L, Zhang C, Fujita M, Li R, Yan SM, *et al*. Genomic and transcriptomic profiling of combined hepatocellular and intrahepatic cholangiocarcinoma reveals distinct molecular subtypes. Cancer Cell 2019;35(6):932-47.e8.
93. Klco JM, Miller CA, Griffith M, Petti A, Spencer DH, Ketkar-Kulkarni S, *et al*. Association between mutation clearance after induction therapy and outcomes in acute myeloid leukemia. JAMA 2015;314(8):811-22.
94. Sazonova EV, Kopeina GS, Imyanitov EN, and Zhivotovsky B. Platinum drugs and taxanes: can we overcome resistance? Cell Death Discov 2021;7(1):155.
95. Wang L, Zhao X, Fu J, Xu W, and Yuan J. The role of tumour metabolism in cisplatin resistance. Front Mol Biosci 2021;8:691795.
96. Hientz K, Mohr A, Bhakta-Guha D, and Efferth T. The role of p53 in cancer drug resistance and targeted chemotherapy. Oncotarget 2017;8(5):8921-46.
97. Sazonova EV, Kopeina GS, Imyanitov EN, and Zhivotovsky B. Platinum drugs and taxanes: can we overcome resistance? Cell Death Discov 2021;7(1):155.
98. Reed E. Platinum-DNA adduct, nucleotide excision repair and platinum based anti-cancer chemotherapy. Cancer Treat Rev 1998;24(5):331-44.
99. Zervantonakis IK, Iavarone C, Chen HY, Selfors LM, Palakurthi S, Liu JF, *et al*. Systems analysis of apoptotic priming in ovarian cancer identifies vulnerabilities and predictors of drug response. Nat Commun 2017;8(1):365.
100. Zhou J, Kang Y, Chen L, Wang H, Liu J, Zeng S, *et al*. The drug-resistance mechanisms of five platinum-based antitumor agents. Front Pharmacol 2020;11:343.
101. Huang D, Savage SR, Calinawan AP, Lin C, Zhang B, Wang P, *et al*. A highly annotated database of genes associated with platinum resistance in cancer. Oncogene 2021;40(46):6395-405.
102. Li X, Chen W, Jin Y, Xue R, Su J, Mu Z, *et al*. miR-142-5p enhances cisplatin-induced apoptosis in ovarian cancer cells by targeting multiple anti-apoptotic genes. Biochem

Pharmacol 2019;161:98-112.
103. Seki K, Yoshikawa H, Shiiki K, Hamada Y, Akamatsu N, and Tasaka K. Cisplatin (CDDP) specifically induces apoptosis via sequential activation of caspase-8, -3 and -6 in osteosarcoma. Cancer Chemother Pharmacol 2000;45(3):199-206.
104. Vogt PK and Hart JR. PI3K and STAT3: a new alliance. Cancer Discov 2011;1(6):481-6.
105. Liang F, Ren C, Wang J, Wang S, Yang L, Han X, *et al*. The crosstalk between STAT3 and p53/RAS signaling controls cancer cell metastasis and cisplatin resistance via the Slug/MAPK/PI3K/AKT-mediated regulation of EMT and autophagy. Oncogenesis 2019;8(10):59.
106. Marabelle A, Le DT, Ascierto PA, Di Giacomo AM, De Jesus-Acosta A, Delord JP, *et al*. Efficacy of pembrolizumab in patients with noncolorectal high microsatellite instability/mismatch repair-deficient cancer: results from the phase II KEYNOTE-158 study. JCO 2020;38(1):1-10.
107. Momoi H, Itoh T, Nozaki Y, Arima Y, Okabe H, Satoh S, *et al*. Microsatellite instability and alternative genetic pathway in intrahepatic cholangiocarcinoma. J Hepatol 2001;35(2):235-44.
108. Isa T, Tomita S, Nakachi A, Miyazato H, Shimoji H, Kusano T, *et al*. Analysis of microsatellite instability, K-ras gene mutation and p53 protein overexpression in intrahepatic cholangiocarcinoma. Hepatogastroenterology 2002;49(45):604-8.
109. Agaram NP, Shia J, Tang LH, and Klimstra DS. DNA mismatch repair deficiency in ampullary carcinoma: a morphologic and immunohistochemical study of 54 cases. Am J Clin Pathol 2010;133(5):772-80.
110. Moy AP, Shahid M, Ferrone CR, Borger DR, Zhu AX, Ting D, *et al*. Microsatellite instability in gallbladder carcinoma. Virchows Arch 2015;466(4):393-402.
111. Bonneville R, Krook MA, Kautto EA, Miya J, Wing MR, Chen HZ, *et al*. Landscape of microsatellite instability across 39 cancer types. JCO Precis Oncol 2017;2017:PO.17.00073.
112. Salem ME, Puccini A, Grothey A, Raghavan D, Goldberg RM, Xiu J, *et al*. Landscape of tumor mutation load, mismatch repair deficiency, and PD-L1 expression in a large patient cohort of gastrointestinal cancers. Mol Cancer Res 2018;16(5):805-12.
113. Ueno M, Chung HC, Nagrial A, Marabelle A, Kelley RK, Xu L, *et al*. Pembrolizumab for advanced biliary adenocarcinoma: results from the multicohort, phase II KEYNOTE-158 study. Ann Oncol 2018;29:viii210.
114. Trigg RM, Martinson LJ, Parpart-Li S, and Shaw JA. Factors that influence quality and yield of circulating-free DNA: a systematic review of the methodology literature. Heliyon 2018;4(7):e00699.
115. Hodi FS, Wolchok JD, Schadendorf D, Larkin J, Long GV, Qian X, *et al*. TMB and inflammatory gene expression associated with clinical outcomes following immunotherapy in advanced melanoma. Cancer Immunol Res 2021;9(10):1202-13.
116. McGrail DJ, Pilié PG, Rashid NU, Voorwerk L, Slagter M, Kok M, *et al*. High tumor mutation burden fails to predict immune checkpoint blockade response across all cancer types. Ann Oncol 2021;32(5):661-72.
117. Sha D, Jin Z, Budczies J, Kluck K, Stenzinger A, and Sinicrope FA. Tumor mutational burden as a predictive biomarker in solid tumors. Cancer Discov 2020;10(12):1808-25.
118. Wu HX, Wang ZX, Zhao Q, Chen DL, He MM, Yang LP, *et al*. Tumor mutational and indel burden: a systematic pan-cancer evaluation as prognostic biomarkers. Ann Transl Med 2019;7(22):640.

119. Jiang T, Chen J, Xu X, Cheng Y, Chen G, Pan Y, *et al*. On-treatment blood TMB as predictors for camrelizumab plus chemotherapy in advanced lung squamous cell carcinoma: biomarker analysis of a phase III trial. Mol Cancer 2022;21(1):4.
120. Neumann O, Burn TC, Allgäuer M, Ball M, Kirchner M, Albrecht T, *et al*. Genomic architecture of FGFR2 fusions in cholangiocarcinoma and its implication for molecular testing. Br J Cancer 2022;127(8):1540-49.
121. Bekaii-Saab TS, Bridgewater J, and Normanno N. Practical considerations in screening for genetic alterations in cholangiocarcinoma. Ann Oncol 2021;32(9):1111-26.
122. Goyal L, Saha SK, Liu LY, Siravegna G, Leshchiner I, Ahronian LG, *et al*. Polyclonal secondary FGFR2 mutations drive acquired resistance to FGFR Inhibition in patients with FGFR2 fusion-positive cholangiocarcinoma. Cancer Discov 2017;7(3):252-63.
123. Berchuck JE, Facchinetti F, DiToro DF, Baiev I, Majeed U, Reyes S, *et al*. The clinical landscape of cell-free DNA alterations in 1671 patients with advanced biliary tract cancer. Ann Oncol 2022;33(12):1269-83.

APPENDICES

APPENDICE A. Gene list of TMB500 panel

Gene						
ABL1	*ABL2*	*ACVR1*	*ACVR1B*	*PARP1*	*AKT1*	*AKT2*
BIRC3	*FAS*	*AR*	*ARAF*	*RHOA*	*ZFHX3*	*ATF1*
AXL	*B2M*	*BARD1*	*CCND1*	*BCL2*	*BCL2L1*	*BCL6*
BMPR1A	*FOXL2*	*BRCA1*	*BRAF*	*BRCA2*	*BTK*	*BUB1B*
RUNX1	*RUNX1T1*	*CBFB*	*CBL*	*CBLB*	*CCND2*	*CCND3*
CD79A	*CD79B*	*CDH1*	*CDK4*	*CDK6*	*CDK8*	*CDKN1A*
CDKN2C	*CEBPA*	*CFTR*	*CHD4*	*CHEK1*	*KLF6*	*CREBBP*
CTLA4	*CTNNA1*	*CTNNB1*	*CUX1*	*CYLD*	*CYP1B1*	*CYP2C8*
DAXX	*DNMT3A*	*DPYD*	*EGFR*	*EIF1AX*	*EP300*	*EPHA3*
EPHB4	*ERBB2*	*ERBB3*	*ERBB4*	*ERCC1*	*ERCC2*	*ERCC3*
ERG	*ESR1*	*ETS1*	*ETV1*	*ETV4*	*ETV5*	*ETV6*
EZH2	*FANCA*	*FANCC*	*FANCD2*	*FANCE*	*FANCF*	*FANCG*
FGF3	*FGF4*	*FGF5*	*FGF6*	*FGF7*	*FGF8*	*FGF9*
FGFR1	*FGFR3*	*FGFR2*	*FGFR4*	*FH*	*FOXO1*	*FOXO3*
FLT4	*FN1*	*MTOR*	*FYN*	*G6PD*	*GABRA6*	*GATA1*
GATA6	*GLI1*	*GNA11*	*GNAQ*	*GNAS*	*GPS2*	*GRIN2A*
HDAC1	*HGF*	*NRG1*	*HLA-A*	*HLA-B*	*HLA-C*	*HLF*
HSP90AB1	*DNAJB1*	*ID3*	*IDH1*	*IDH2*	*IGF1*	*IGF1R*
IL2	*IL6ST*	*IL7R*	*IL10*	*INHA*	*INHBA*	*INPP4A*
IRF4	*IRS1*	*JAK1*	*JAK2*	*JAK3*	*JUN*	*KDR*
LAMP1	*LCK*	*LMO1*	*LYN*	*SH2D1A*	*EPCAM*	*SMAD2*
MAX	*MCL1*	*MDM2*	*MDM4*	*MAP3K1*	*MEN1*	*MET*
AFF1	*MLLT3*	*MPL*	*MRE11*	*MSH2*	*MSH3*	*MSI1*
MUTYH	*MYC*	*MYCL*	*MYCN*	*MYD88*	*MYH11*	*MYOD1*
NFE2L2	*NFKBIA*	*NKX3-1*	*NOTCH1*	*NOTCH2*	*NOTCH3*	*NOTCH4*
NTRK1	*NTRK2*	*NTRK3*	*DDR2*	*NUMA1*	*NUP98*	*PAK1*
PDGFB	*PDGFRA*	*PDGFRB*	*PGR*	*PIK3C2B*	*PIK3C2G*	*PIK3C3*
PIK3CD	*PIK3CG*	*PIK3R1*	*PIK3R2*	*PLCG2*	*PML*	*PMS1*
PPARG	*PPP2R1A*	*PPP2R2A*	*PPP6C*	*PRKAR1A*	*PRKCI*	*PRKDC*

MAP2K2	*PRSS1*	*PTCH1*	*PTEN*	*PTGS2*	*PTPN11*	*PTPRD*
RAD51	*RAD51C*	*RAD51B*	*RAD51D*	*RAD52*	*RAF1*	*RARA*
REL	*RET*	*RHEB*	*RIT1*	*ROS1*	*RPS6KB2*	*RXRA*
SDHD	*MAP2K4*	*SRSF2*	*SHH*	*SMARCA4*	*SMARCB1*	*SMO*
SPINK1	*SRC*	*SSX1*	*STAT3*	*STAT4*	*STAT5A*	*STAT5B*
TAF1	*TAL1*	*TAP2*	*TBX3*	*HNF1A*	*TCF3*	*TCF7L2*
TGFBR1	*TGFBR2*	*TIMP3*	*NKX2-1*	*TLR4*	*TMPRSS2*	*TNFAIP3*
XPC	*NUP214*	*TP63*	*TP53BP1*	*SMC1A*	*RPS6KA4*	*PDE4DIP*
XPO1	*MLLT10*	*SOCS1*	*TRAF2*	*ARID1A*	*LATS1*	*DEPDC5*
XRCC2	*FGF23*	*IRS2*	*TSC1*	*AXIN1*	*SMC3*	*NUP93*
YES1	*KMT2D*	*EED*	*TSC2*	*AXIN2*	*AURKB*	*KMT2B*
ZNF217	*TCL1A*	*TNFRSF14*	*TSHR*	*BAP1*	*KLF4*	*KEAP1*
PAX8	*NPRL3*	*INPP4B*	*U2AF1*	*SPOP*	*RECQL4*	*GAB2*
CXCR4	*NCOA3*	*STK19*	*KDM6A*	*RAD54L*	*QKI*	*MAGI2*
DEK	*ZRSR2*	*FUBP1*	*VEGFA*	*CUL3*	*NCOR1*	*MAFB*
KAT6A	*RBM10*	*BCL10*	*VHL*	*PPM1D*	*IKBKE*	*FGF19*
BRD3	*KDM5C*	*PHOX2B*	*NSD2*	*PIK3R3*	*MDC1*	*MED12*
PBRM1	*PREX2*	*ASXL1*	*WRN*	*CARD11*	*BCORL1*	*AKT3*
FANCI	*TET1*	*ARID2*	*WT1*	*DOT1L*	*CRLF2*	*BCL2L11*
ASXL2	*PDCD1LG2*	*FLCN*	*XPA*	*SLX4*	*SOX17*	*SH2B3*
FBXW7	*CD276*	*RICTOR*	*PALB2*	*KLHL6*	*NSD1*	*PARP2*
EMSY	*TCF7L1*	*NUTM1*	*ZNF703*	*KNSTRN*	*BCL11B*	*PARP3*
CYSLTR2	*BRIP1*	*NEGR1*	*MEF2B*	*FOXP4*	*CDC73*	*RAD50*
ARID1B	*ARID5B*	*GEN1*	*WISP3*	*AMER1*	*VTCN1*	*RPTOR*
KMT2C	*ALK*	*ALOX12B*	*APC*	*ATM*	*ATR*	*ATRX*
BCR	*PRDM1*	*BLM*	*TOP1*	*TOP2A*	*TP53*	*SMAD3*
DDR1	*CALR*	*CASP8*	*STAG1*	*MGA*	*CD274*	*MITF*
CCNE1	*CD22*	*CD70*	*IKZF1*	*ICOSLG*	*IL21R*	*MST1R*
CDKN1B	*CDKN2A*	*CDKN2B*	*YAP1*	*CRTC1*	*ING4*	*NBN*
CRKL	*CSF1R*	*CSF3R*	*CARM1*	*DICER1*	*FZR1*	*NPM1*
CYP2D6	*CYP3A4*	*CYP3A5*	*CTCF*	*SF3B1*	*DDX41*	*PAX5*
EPHA5	*EPHA7*	*EPHB1*	*STAG2*	*BRD4*	*SUFU*	*PIK3CA*

ERCC4	*ERCC5*	*ERF*	*PLK2*	*SUZ12*	*CDK12*	*PMS2*
EWSR1	*EXT1*	*EXT2*	*FRS2*	*KAT6B*	*ERRFI1*	*MAPK1*
FAT1	*FGF1*	*FGF2*	*MALT1*	*SETBP1*	*INO80*	*PTPRS*
FGF10	*FGF12*	*FGF14*	*PNRC1*	*LATS2*	*UGT1A1*	*RASA1*
FLI1	*FLT1*	*FLT3*	*PTPRT*	*MLH3*	*TET2*	*SDHA*
GATA2	*GATA3*	*GATA4*	*CHEK2*	*FOXP1*	*SAMD9*	*SOS1*
GRM3	*GSK3B*	*MSH6*	*RRAS2*	*AGO2*	*BCOR*	*AURKA*
FOXA1	*HRAS*	*HSP90AA1*	*DIS3*	*EML4*	*RNF43*	*TEK*
IGF2	*IGF2R*	*IKBKB*	*SPEN*	*SETD2*	*NSD3*	*SMAD4*
INPPL1	*INSR*	*IRF2*	*CIC*	*ANKRD11*	*FANCL*	*MLH1*
KIF5B	*KIT*	*KRAS*	*TRAF7*	*SPRED1*	*PHF6*	*MTAP*
MAF	*NF1*	*NF2*	*PIK3CB*	*POLE*	*RB1*	*SDHC*
KMT2A	*NRAS*	*NTHL1*	*POLD1*	*MAP2K1*	*SDHB*	*SOX9*
MUC1	*PBX1*	*PDCD1*	*MAPK3*	*RAD21*	*SOX2*	*SYK*
TERT	*TFE3*	*PIM1*	*RAC1*	*KDM5A*	*STK11*	

APPENDICE B. Detected PDR genes

Associated Pathway	Detected PDR genes
TP53 signaling	*TP53, ATM, CDKN1A, CDKN2A*
DNA repair (NER, HR, and MMR)	*ERCC1, BRCA1, MSH6*
PI3K pathway	*PIK3CA, PIK3CB, PIK3CD, PIK3R1*
Cell death	*BCL2, BIRC3, CASP8*
MAPK pathway	*MAPK1, MAPK3*
ERBB pathway	*ERBB2*

ABSTRACT(IN KOREAN)

화학적 항암치료를 받는 담도암 환자에게서 순환 종양 DNA의 중요성

<지도교수 최종락>

연세대학교 대학원 의과학과

윤 우 빈

담도암은 담즙이 배출되는 경로인 담관, 담낭에서 유발되는 악성 종양을 일컫는다. 서구권보다는 동양권에서 발생 빈도가 매우 높게 관찰되며, 최근 연구들에 의하면, 이러한 경향은 유지되나 전세계적으로 발생빈도 증가하는 것으로 알려져 있다. 발병 위치에 따라 유전적 특성이 서로 다르게 띄는 종양 이질성 (tumor heterogeneity)을 특성으로 하며, 아직 명확한 치료법이 없는 것으로 알려져 있으며, 수술을 통한 절제술만이 완치를 기대할 수 있는 유일한 치료법이다. 대부분의 담도암 환자들은 초기 증상이 없어 수술이 불가능한 말기 상태에서 진단되며, 이로 인해 매우 낮은 생존률을 보이는 암종이다. 암 진단을 위해 조직생검이 일반적으로 시행되나, 침습적 방식으로 인해 일부 한계점이 지적되어 왔다. 액체 생검은 이를 보완할 수 있는 수단으로 매우 각광받는 받고 있다. 하지만 이를 이용한 국내외의 연구들은 임상적 필요성을 충족하지 못하는 실정이다. 본 연구에서는 전향적으로 구성된 41명의 고식적 화학 항암치료를 받은 담도암 환자들을 1차, 2차, 4차 항암치료 전 그리고 암의 진행 (progression disease) 단계에서 채혈을 통해 얻은 순환 종양 DNA의 유전정보를 분석하여 약물 반응 감시, 치료 가능 유전자 발굴, 담도암에 대한 분자적 기전 이해를 높이고자 한다.

핵심되는 말 : 담도암, 화학적 항암치료, 세포 유리 DNA, 순환 종양 DNA, 차세대 염기서열 분석법, 액체생검